NBSIR 83-2641

The Application of Laser-Induced Rayleigh Light Scattering to the Study of Turbulent Mixing

U.S. DEPARTMENT OF COMMERCE
National Bureau of Standards
National Engineering Laboratory
Center for Fire Research
Washington, DC 20234

January 1983

U.S. DEPARTMENT OF COMMERCE
NATIONAL BUREAU OF STANDARDS

NBSIR 83-2641

THE APPLICATION OF LASER-INDUCED RAYLEIGH LIGHT SCATTERING TO THE STUDY OF TURBULENT MIXING

William M. Pitts
Takashi Kashiwagi

U.S. DEPARTMENT OF COMMERCE
National Bureau of Standards
National Engineering Laboratory
Center for Fire Research
Washington, DC 20234

January 1983

U.S. DEPARTMENT OF COMMERCE, Malcolm Baldrige, *Secretary*
NATIONAL BUREAU OF STANDARDS, Ernest Ambler, *Director*

Table of Contents

		Page
List of Figures		v
List of Tables		viii
Nomenclature		ix
Abstract		1
1.	INTRODUCTION	2
1.1	Preliminary Remarks	2
1.2	Scalar Measurement Techniques in Turbulent Flow Fields	4
2.	RAYLEIGH SCATTERING	13
2.1	Description of Rayleigh Scattering	13
2.2	Past Uses of Rayleigh Scattering as a Probe in Turbulent Flow Systems	17
2.3	Expected Signal and Noise Levels for Rayleigh Scattering Measurements	19
3.	TURBULENCE MEASUREMENTS	26
3.1	Nature of Turbulence and Approaches to its Characterization	26
3.2	Calculational Methods for Properties of the Concentration Flow Field	28
4.	EQUIPMENT AND PROCEDURES	36
4.1	Flow System	36
4.2	Optical System	38
4.3	Detection, Conditioning, and Recording Electronics	39
4.4	Experimental Procedures	41
4.5	Data Analysis	42
5.	RESULTS	46
5.1	Nature of Detected Rayleigh Scattering	46
5.2	Time Averaged Properties of the Methane Concentration Field	48
5.3	Conditional Measurements in the Methane Concentration Field	54
6.	DISCUSSION	58
6.1	Comparisons of Measurements from this Study with Other Work	58
6.2	Validity of Comparisons with Other Studies	70

Page

6.3 Applicability of Rayleigh Light Scattering as a Scalar Probe of Turbulent Flow Fields 73
6.4 Rayleigh versus Raman Scattering as a Scalar Probe 78
6.5 Final Remarks 79

7. ACKNOWLEDGMENTS 80

8. REFERENCES 81

List of Figures

Page

Figure 1. Optical arrangement and detection electronics for laser Rayleigh light scattering measurements 86

Figure 2. Detected light intensity as a function of position for a back-illuminated pinhole translated along the laser beam propagation direction. The symbols represent data for 0.2 mm (X) and 0.4 mm (◇) slit widths 87

Figure 3. Appearance of data records for time-resolved light scattering measurements as a function of cut-off frequency. The measurement volume is located on the jet axis at $z/r_o = 35$. The vertical axis indicates methane concentrations which are uncorrected for photon statistics. Average methane concentrations for the entire data sets are indicated by X and the expected RMS fluctuations ($\pm$ 1 σ) due only to photon statistics are indicated by the bars 88

Figure 4. Values of $\left(\bar{X}_{CH_4}\right)_o / \left(\bar{X}_{CH_4}\right)_c$ and $\left(\bar{Y}_{CH_4}\right)_o / \left(\bar{Y}_{CH_4}\right)_c$ are plotted as a function of z/r_o. Solid lines are the results of linear least squares fits for measurements taken at $z/r_o \geq 20$ 89

Figure 5. Values of $\left(\bar{X}_{CH_4}\right)_o / \left(\tilde{X}_{CH_4}\right)_c$ and $\left(\bar{Y}_{CH_4}\right)_o / \left(\tilde{Y}_{CH_4}\right)_c$ are plotted as a function of z/r_o. Solid lines are the results of linear least squares fits for measurements taken at $z/r_o \geq 20$ 90

Figure 6. Unmixedness of methane concentration on the jet centerline in mole and mass fraction terms is plotted as a function of z/r_o 91

Figure 7. The skewness of the methane concentration distribution on the jet centerline is plotted as a function of z/r_o 92

Figure 8. The kurtosis of the methane concentration distribution on the jet centerline is plotted as a function of z/r_o 93

Figure 9. Examples of correlation functions and power spectra for methane concentration fluctuations at three different axial downstream distances in a methane-air jet. The cut-off frequency of the amplifier is set to 4.6 kHz 94

Page

Figure 10. Integral time scales (T) on the jet centerline as a function of z/r_o 95

Figure 11. Behaviors of $\bar{X}_{CH_4}$ and $\bar{Y}_{CH_4}$ are shown as a function of nondimensionalized radial distance ($r/r_{1/2}$) for a downstream distance of $z/r_o = 35$ in a methane-air jet. Solid lines are results for fits of Eq. (5.5) ... 96

Figure 12. Experimental values of $\tilde{X}_{CH_4}/\left(\tilde{X}_{CH_4}\right)_c$ and $\tilde{Y}_{CH_4}/\left(\tilde{Y}_{CH_4}\right)_c$ are shown as a function of nondimensionlized radial distance ($r/r_{1/2}$) for a downstream distance of $z/r_o = 35$ in a methane-air jet. The solid line represents results taken from the work of Becker et al. [48] for an air-air jet and the dashed line gives the results of Birch et al. [23] for a methane-air jet 97

Figure 13. Skewness values as a function of nondimensionalized radial distance ($r/r_{1/2}$) are shown for the methane concentration distribution at a downstream distance $z/r_o = 35$ in a methane-air jet. Values have been calculated for entire data records (◈) and for conditionally sampled data which are weighted by the corresponding intermittency functions (X) 98

Figure 14. Kurtosis values as a function of nondimensionalized radial distance ($r/r_{1/2}$) are shown for the methane concentration distribution at a downstream distance $z/r_o = 35$ in a methane-air jet. Values have been calculated for entire data records (◈) and for conditionally sampled data which are weighted by the corresponding intermittency functions (X) 99

Figure 15. Integral time scales as a function of nondimensionalized radial distance ($r/r_{1/2}$) are shown for methane concentration fluctuations at a downstream distance $z/r_o = 35$ in a methane-air jet 100

Figure 16. Example of methane concentration behavior in the intermittent region of a methane-air jet and the resulting intermittency function calculated for the data. Arrows indicate short "bursts" of methane concentration which do not appear in the intermittency function due to the averaging inherent in the calculation of this function..... 101

Figure 17. Intermittency factor (γ) and frequency (f_γ) as functions of nondimensionalized radial distance

$(r/r_{1/2})$ for a downstream distance of $z/r_o = 35$ in a methane-air jet. The solid line is a plot of Eq. (5.6) for $\bar{R} = 1.6\ r_{1/2}$ and $\sigma_w = .28\ r_{1/2}$ 102

Figure 18. Values of the intermittency factor (γ) are plotted on a probability graph as a function of nondimensionalized radial distance $(r/r_{1/2})$. The solid line is a linear least square fit of all results except the five points closest to the jet centerline. The symbols refer to positive (◈) and negative (⊡) values of r 103

Figure 19. Plots of $\bar{X}_{CH_4}$ and $\tilde{X}_{CH_4}/(\tilde{X}_{CH_4})_c$ are given as a function of the nondimensionalized radial distance $r/r_{1/2}$ at a downstream distance $z/r_o = 35$ in a methane-air jet. The corresponding conditionally sampled values, $(\bar{X}_{CH_4})_T$ and $(\tilde{X}_{CH_4})_T/(\tilde{X}_{CH_4})_c$, are indicated by the symbol X 104

List of Tables

Page

Table 1. Observed and calculated relative errors as a function of cut-off frequency for the current from a photomultiplier illuminated by a constant intensity light source 105

Table 2. Experimentally determined constants for Eqs. (5.1)-(5.4) and asymptotic values for concentration fluctuation intensity on the jet centerline in mole and mass fraction terms 106

Table 3. Observed constants for spreading rate behavior (Eq. 6.1) of axisymmetric jets 107

Table 4. Maximum normalized RMS concentration fluctuation values and radial locations for various axisymmetric jets 108

Table 5. Experimental parameters for different jets discussed in text 109

Nomenclature

B	dummy variable
C_1^X, C_1^Y, C_2^X, C_2^Y	constants for Eqs. (5.1) - (5.4)
C_3	constant for Eq. (6.1)
Ct	Craya-Curtet number
D	jet exit diameter
f_γ	intermittency frequency
fl	focal length
G	gain of photomultiplier tube
i	photomultiplier current output
i_{AVG}	average photomultiplier current output during $\Delta t'$
I	total light intensity scattered from two component gas
I_L	laser output (photons/s)
I_o	laser irradiance (W cm^{-2}) incident on observation volume
$I_\parallel$	intensity (W sr^{-1} cm^{-3}) of light scattered from a unit observation volume which is parallel to the electric field of incident polarized light
$I_\perp$	intensity (W sr^{-1} cm^{-3}) of light scattered from a unit observation volume which is perpendicular to the electric field of incident polarized light
I(t)	intermittency function
K	kurtosis (flatness)
l	length of cylindrical observation volume
L	number of measurements
M	number of gases in a mixture
n	index of refraction
N	number density of gas
N_o	Avogadro's number
N_P	number of photons detected

P	pressure
q_t	integrated current (charge) during Δt
q_t'	integrated current (charge) during $\Delta t'$
r	radial distance from jet centerline
$r_{1/2}$	radial distance at which concentration has fallen to 0.5 of centerline value
r_ε	effective radius
R	gas constant; instantaneous distance from outside edge of jet to centerline
$\bar{R}$	value of R for $\gamma = 0.5$
Re	Reynolds number
R_P	rate of photon detection
$R(\tau)$	correlation function
S	skewness
t	time
T	temperature
u	velocity
X	mole fraction
X'	measurement of mole fraction in presence of shot noise
Y	mass fraction
z	axial downstream distance from jet nozzle exit
z_o	virtual origin
α	gain per dynode in photomultiplier
α_ρ	density ratio - 1
γ	intermittency factor
Δf	bandpass of cut-off frequency filter
Δt	time period
$\Delta t'$	effective integration time when a cut-off frequency filter is used

ε	quantum yield of photomultiplier
η_C	coefficient of optical transmission between observation volume and detector
η_L	coefficient of optical transmission between the laser and observation volume
λ	wavelength
μ_r	rth central moment
μ'_r	rth moment
$\mu_{(r)}$	rth central factorial moment
$\mu'_{(r)}$	rth factorial moment
ν	kinematic viscosity
ξ	unmixedness
σ	angular cross section ($cm^2\ sr^{-1}$) for Rayleigh light scattering
σ_a	90^o scattering cross section for air
σ_f	90^o scattering cross section for fuel
σ_w	wrinkle amplitude
ρ	density; depolarization ratio
τ	dummy variable for autocorrelation
T	integral time scale
ω	frequency
Ω	solid angle for light collection
$\Phi(\omega)$	power spectrum

Superscripts

a	anisotropic
i	isotropic
$\bar{B}$	average value of B for L measurements
$\tilde{B}$	RMS for fluctuations of B for L measurements

Subscripts

a	value for air
f	value for fuel (jet gas)
j	index for summation
PC	photocount
PF	photon field
air	value for air
CH_4	value for methane
tur	value for turbulent flow
$(B)_c$	value of B on jet centerline
$(B)_o$	value of B at jet exit
$(B)_T$	conditionally sampled value of B in turbulent region only
$(B)_{max}$	largest value of B in radial direction

The Application of Laser-Induced Rayleigh Light Scattering to the Study of Turbulent Mixing

Abstract

This work describes the development and characterization of an experimental system employing laser-induced Rayleigh light scattering with digital data acquisition as a time-resolved, quantitative concentration probe in the turbulent flow field of a binary gas mixture. Equations for the expected signal and noise levels are given. Estimates of these parameters for the experimental system used here are in satisfactory agreement with experiment. It is demonstrated that the laser Rayleigh light scattering technique provides measurements having high spatial and temporal resolution for various locations within the concentration flow field. Measurements at various positions in the flow field of an axisymmetric methane jet issuing into a slow flow of air are reported and, where possible, compared with appropriate literature results. The statistical properties of the turbulent concentration fluctuations are found to be in good agreement with other independent measurements. Conditionally sampled measurements are also reported and shown to behave in the same manner as the limited number of similar measurements in the literature. The capability of calculating power spectra and correlation functions for the time behavior of the methane concentration is also demonstrated. Other techniques employed for scalar measurements in turbulent flow fields are briefly reviewed and the utility of these techniques for

measurements in different types of flow systems are discussed in relation to the Rayleigh light scattering method.

Key words: Axisymmetric jets; flow fields; intermittency; lasers; ramp-like structures; Rayleigh scattering; scalars; turbulence; turbulent flow.

1. INTRODUCTION

1.1 Preliminary Remarks

Despite years of study, a full understanding of turbulent behavior remains elusive. This is unfortunate since turbulence occurs in many natural and man-made systems. Turbulent flow is the most effective means of mixing two or more fluids, and for this reason it is especially important in combustion and reaction systems where mixing must precede molecular interactions. For this reason, understanding chemically reacting turbulent flows is a key to the more effective utilization of natural resources and the control of pollution. Development of effective turbulence models is essential for the design and construction of systems which utilize turbulent mixing most effectively. An understanding of this phenomenon is so critical that turbulence is often said to be the most important unsolved problem in physics.

We have initiated an experimental program with the long term goal of enhancing the fundamental understanding of chemically reacting turbulent flow. Our goal is to generate detailed data which can be used to empirically describe the behavior of such flows and to provide input for mathematical models designed to predict their behavior. An approach to the problem has

been chosen in which the effects of changes in density and temperature on turbulent behavior are first isolated and evaluated for a well defined and widely studied flow configuration. Once the effects of changes in these parameters are understood, it will be possible to isolate the effects of the nonlinear coupling which occurs between a turbulent flow and a chemically reacting system.

The need for an accurate, time-resolved probe of concentration in the turbulent flow field led us to evaluate several experimental techniques for their effectiveness for such measurements. These included obtrusive probes, such as those using hot-wires, and more modern nonobtrusive optical techniques such as marker nephelometry, Raman scattering, and Rayleigh scattering. A discussion of the advantages and disadvantages of many of these techniques is included in Section 1.2. Based on our analysis, we have chosen laser-induced Rayleigh light scattering as the technique most suited to our particular measurement requirements. This decision is based on the relative sensitivity of the technique and its ability to perform nonobtrusive measurements with high temporal and spatial resolution.

There have been two past studies reported in the literature which indicated that Rayleigh light scattering might be a suitable probe of concentration behavior in turbulent flow systems [1,2].[1] This report describes the development of such a system and how it is used to perform scalar measurements and includes a detailed analysis of the spatial and temporal resolution which can be achieved. A wide variety of properties of

[1]Numbers in brackets indicate the literature references at the end of the paper.

the behavior of concentration fluctuations for an axisymmetric turbulent jet of methane issuing into air are reported and compared with similar measurements available in the literature. The conclusion of this report is that, for certain types of flows, Rayleigh scattering is an extremely powerful technique for turbulent flow field scalar measurements.

In the following section (Section 2) the Rayleigh effect is described and past applications of the technique for concentration, density, and temperature measurements in turbulent systems are reviewed. This section also contains an analysis of expected signal and noise levels. Section 3 describes the nature of concentration fluctuations which occur in a turbulent flow and how the data generated by a Rayleigh scattering experiment are analyzed in order to characterize the concentration field. The experimental system employed for this study is discussed in Section 4. Results of time- and spatially-resolved concentration measurements in the flow field of an axisymmetric turbulent jet of methane issuing into a background flow of air are summarized in Section 5. In the final section (Section 6) these measurements are compared with literature measurements on similar turbulent flows, and the validity of such comparisons is examined. Finally, the usefulness of the Rayleigh scattering technique as a concentration probe of turbulent flow systems is discussed.

1.2 Scalar Measurement Techniques in Turbulent Flow Fields

Those properties of a system which only require a magnitude for their full description (e.g., temperature or concentration) are said to be scalars. Vector properties (e.g., velocity) must be assigned a direction and magnitude. In this work we treat the measurement of scalar values with an emphasis on concentration measurements.

Many different measurement techniques have been used to determine the scalar properties of turbulent flow fields. In this subsection the strengths and weaknesses of some of these techniques will be discussed with a special emphasis on comparison with the Rayleigh light scattering measurements to be described in this work. The following discussion is only illustrative and is not intended to be a detailed review of measurement techniques for scalar properties in turbulent flow fields.

Scalar probes can be classified as obtrusive or nonobtrusive depending on whether or not a physical probe is inserted into the flow field. These two types of probes can be further classified as direct or indirect. A direct probe is defined as one which responds to the property under consideration while an indirect probe is sensitive to a marker present in the flow which is assumed to be passive (i.e., does not change the flow behavior). A probe is said to be specific if it responds to the individual components of a gaseous mixture and nonspecific if it only responds to an overall property of the system such as temperature or density. Another possible trait of scalar probes is their ability to characterize fluctuations in real time. That is, the probe has the ability to repeatedly make determinations of a scalar variable at a frequency sufficiently high that the property appears constant during a time equal to the period of the measurement. Obviously, this period will vary for different flow conditions. The ability to perform real time measurements is important for intermittency and conditionally sampled determinations. All of the probes to be discussed in this section have the capability to make spatially resolved measurements. Using the above definitions, the ideal scalar probe would be nonobtrusive, direct, specific, and capable of infinite temporal and spatial resolution.

Early experiments dealing with the concentration fields of turbulent flows used various obtrusive probes. Usually these studies only reported average values for temperature or concentration. Representative of this early work is that of Hinze and van der Hegge Zijnen [3] who used thermocouples and a capillary connected to a gas analyzer to measure the average temperature and concentration fields of an axisymmetric free jet. Forstall and Shapiro [4] used helium as a passive marker to study the spreading of an axisymmetric jet of air into a coflowing stream of air. Samples were withdrawn from the flow, and the helium content was determined by a standard thermal conductivity cell.

Studies by Corrsin and Uberoi [5,6] showed that hot-wires operated in a low overheat constant current mode could be used to measure average temperature and fluctuation intensities in heated air-air flows. This technique has been widely applied to heated flows with heat acting as a passive marker of concentration changes. Chevray and Tutu [7] extended this early work by using two hot-wires. The first was operated in the low overheat constant current mode to provide a signal proportional to temperature. The second wire was used in the constant current mode which responds to changes in both temperature and velocity. Using the output of the first wire to provide the temperature for the second, the velocity and temperature of the flow could be obtained simultaneously. Much of the current understanding of flow field behavior of axisymmetric jets has come from experiments of this type. Despite the widespread use of these techniques, they often require subtle corrections and questions remain about their performance for flows with large fluctuation intensities.

There have been attempts to extend the use of hot-wires to direct concentration measurements in flows of two gases by Way and Libby [8,9] and McQuaid and Wright [10,11]. In order to perform such measurements, it is necessary to obtain extensive calibrations before collecting actual data and to perform detailed data analysis in order to obtain the final concentration value. The techniques are also subject to the same errors as the hot-wire experiments described above. Due to these problems, these techniques have not been widely applied for concentration measurements.

One additional physical probe method will be mentioned. Brown and Rebollo [12] have described a technique for monitoring the time-resolved concentration fluctuations in a two component gas flow. This technique also uses a hot-wire, but places the wire inside a sampling probe which has an entrance designed to sonically choke the flow so that gas entering passes the hot-wire at a constant velocity and the response of the hot-wire is only to the composition of the gas. By performing extensive calibrations, it is possible to obtain highly accurate measurements of concentration in binary mixtures with high spatial and temporal resolution. It should be noted that the response of the hot-wire to concentration changes is not linear and a fitting procedure is required for converting the recorded signals to concentrations.

The lack of simple, reliable, and universal obtrusive probe methods for scalar measurements in turbulent flows has resulted in efforts aimed at the development of nonobtrusive techniques. Among these techniques are marker nephelometry, Raman and Rayleigh scattering, and electron beam fluorescence. Peterson [13] lists many of the past studies which have used Rayleigh scattering, Raman scattering, and electron-induced fluorescence.

Marker nephelometry is the term given to the technique in which light scattering from particles is used as a probe of concentration fluctuations. Since its introduction in 1961 by Rosensweig et al. [14], this method has proven to be a very useful probe of real-time turbulent fluctuations as manifested by the behavior of small particles seeded into the flow. Becker et al. [15] and Shaughnessy and Morton [16] have described the application of the technique, and Becker [17] has provided a review. There are questions concerning the ability of the particles to follow the flow, and possible coagulation of the particles must be carefully considered. The size of the particles and the seeding levels within the flow must be carefully controlled. Despite these drawbacks, the technique has been applied to a wide range of flow problems which include combustion systems. Recently, the technique has been extended to two dimensions by Long et al. [18]. These workers use a plane of light to illuminate the particles in the flow field. Scattered light is focused on the face of a low-light-level television camera which provides a digitized 2-D image of the field of view. The extension of the scattering technique from a point measurement to 2-D has the potential for providing an improved and highly detailed picture of turbulent mixing. At this stage in its development this technique is not capable of real-time measurements and averages must be made from large numbers of independent measurements.

The Rayleigh scattering technique which is described in this work and marker nephelometry have much in common. Both use light scattering as a probe and for this reason have the potential for high spatial and temporal resolution. Since the Mie scattering used in marker nephelometry is many orders of magnitude stronger than scattering from molecules, the laser employed does not

need to be nearly as powerful as that required for Rayleigh scattering measurements. This advantage is offset somewhat by the requirement to seed the flow with particles. The largest source of noise in the particle scattering technique is marker shot noise. This is a Poisson-type noise which occurs because of the low number of particles in the observation volume. The problem is particularly critical in regions of low concentration. Mie scattering is so strong that electronic shot noise is seldom observed. Since Rayleigh scattering occurs from molecules which are present at high number density ($\sim 2.5 \times 10^{7}\ \mu m^{-3}$), marker shot noise is not a problem, but, as we will show, electronic shot noise due to the weakness of the scattering is the major source of uncertainty in scalar measurements. Marker nephelometry cannot provide temperature information or concentration information for an isothermal tertiary gas mixture, and for this reason is somewhat limited compared to Rayleigh scattering as a turbulence scalar probe. The demonstrated ability of marker nephelometry to be used as a 2-D probe is a significant advance. Our calculations indicate that similar experiments are feasible using Rayleigh scattering as a probe.

The nonspecificity of Rayleigh scattering or marker nephelometry for individual constituents of a gas mixture is a serious drawback to their application in turbulent flows composed of several different gases. The requirement for techniques sensitive to specific components has led to the development of Raman scattering and electron-induced fluorescence as flow field diagnostics.

Raman scattering refers to the inelastic scattering of light by molecules. The energy of the scattered light is shifted from that of the

input source by an amount equal to rotational or vibrational energies of the molecule with which the light is interacting. Since the rotational or vibrational energy spacings of molecules differ, it is possible to resolve the scattered light and identify the molecule with which the light is interacting. The strength of the scattered light is proportional to the number density of the species present. Since the populations of vibrational and rotational levels depend on temperature, it is possible to determine the temperature of gases from the Raman scattering.

The major drawback of the Raman technique is its low intensity. In general, rotational Raman cross sections are ~100 times smaller than Rayleigh cross sections, while vibrational cross sections are ~1000 times smaller. Most experiments use vibrational as opposed to rotational Raman scattering in order to reduce the resolution required to separate the scattered light from the incident light and from the scattering due to different molecules. As we will show in this work, Rayleigh scattering cross sections are just sufficient to obtain time-resolved measurements for turbulent flows with currently available laser sources. It is clear that averaging techniques are necessary in order to apply Raman scattering to scalar measurements in turbulent flow fields.

Two approaches have been adopted in order to obtain the averaged scalar properties of a turbulent flow field using Raman scattering. The first uses high powered pulsed lasers to induce the scattering. A good discussion of this method is found in the review paper of Lederman and Bornstein [19]. The number of photons delivered by these lasers in a time period of 5-20 ns is large enough to ensure that the number of photons which are Raman scattered and detected during a single pulse is sufficient for concentration measure-

ments which have only a few per cent relative error (see discussion in Section 2.3) due to photon statistics. In this manner, a single pulse of the laser is capable of providing a temperature or concentration measurement. Unfortunately, these lasers have repetition rates which vary from 0.1 to several seconds and cannot provide real-time information. In order to obtain accurate characterization of the average properties of the flow field, thousands of measurements are repeated and the results are used to obtain averages, standard deviations, and higher moments of the fluctuating property which is being investigated. The technique is not capable at its current level of development of providing temporal information for such quantities as spectral densities, intermittency functions, or conditionally sampled measurements. The extent of development of the technique is probably best represented by the work of Drake et al. [20] who have simultaneously monitored temperature and nitrogen, hydrogen, and water concentrations in turbulent diffusion flames. Recently, Webber et al. [21] have demonstrated that two-dimensional measurements can be made using Raman scattering induced by a pulsed laser and imaged onto the face of a low-light-level television camera.

It has been known for a long time that Raman scattering induced by a CW laser can be used to obtain the average concentration of individual components within a flow field by collecting the scattering for a long period of time. However, it was believed that the weakness of the scattering precluded a determination of the fluctuation behavior. Birch et al. [22,23] have developed a technique which allows repeated measurements of Raman scattering for short periods of time to yield this information despite the fact that the number of photons detected during any single period is so low that the individual concentration measurements are essentially meaningless. The first

paper by these authors described a photon correlation method which allowed a determination of the average, RMS, and autocorrelation of concentration fluctuations in a methane jet. In a second report they introduced the concepts used in Section 3.2 to deconvolute the effects of photon statistics from concentration measurements. These concepts are valid for the Raman effect even though the effect is 1000 times weaker than Rayleigh scattering. By the use of this method, these authors have been able to map out many of the time-averaged properties of a methane-air jet. This work must be considered a breakthrough in attempts to apply Raman scattering as a diagnostic for turbulent flow systems.

The electron-beam fluorescence technique is a nonobtrusive method which can be considered to be an analog to both Rayleigh and Raman light scattering. The light source is replaced by an electron beam and the detected light arises from atoms or molecules which are electronically excited by the electrons. The technique is selective since fluorescence from different atoms or molecules occurs at different wavelengths which can be resolved. The paper by Smith and Driscoll [24] contains a good description of the technique and the signal levels which are expected as density and temperature are changed. The technique is capable of generating photon detection rates which are sufficient to perform accurate concentration measurements at rates up to several hundred kHz. Unfortunately, due to the collisional quenching of fluorescence which occurs at higher pressures, the technique is only suitable for low density flows. As pressures approach atmospheric, quenching causes severe problems in signal levels and calibration. These considerations indicate that the electron-beam fluorescence technique will be the method of choice when the density is low. As such, it complements Raman and Rayleigh scattering scalar measurements which are best used in higher pressure regimes.

2. RAYLEIGH SCATTERING

2.1 Description of Rayleigh Scattering

The following discussion of Rayleigh scattering considers the special case of a vertically polarized laser beam passing through a gas. A suitable detector of scattered light is located perpendicular to the propagation direction of the laser and the electric field direction of the light. The collection optics of the detector are stopped down in such a manner that it observes only a small volume of space containing the laser beam. This hypothetical arrangement is very similar to that actually used in most experiments, including the one reported here. We now give equations describing the intensity and polarization behavior of scattered radiation reaching the detector. An excellent discussion of Rayleigh light scattering is given in the book by McCartney [25].

For the purpose of this work we have assumed that the effects of rotational Raman scattering are negligible since the cross section for this process is ~ 100 times smaller than that for Rayleigh scattering. It should be noted that it may be necessary to include Raman effects in order to accurately predict observed depolarization ratios.

Rayleigh scattering refers to elastic (no shift in frequency) scattering of electromagnetic radiation which occurs when the electric field of the radiation interacts with the electric fields of atoms or molecules. In this case, we will be interested in visible light, but the equations are also valid for radiation in the infrared and ultraviolet. The oscillating electric field

associated with the electromagnetic radiation induces an oscillating electric dipole moment within the individual atoms or molecules which constitute the gas. These induced dipoles generate additional electromagnetic waves which can propagate in a direction different from that in which the light was originally traveling. These new waves are the scattered light. The strength of the induced dipole and hence the intensity of the scattered light can be directly related to the polarizability of the molecule with which the radiation interacts. The polarizabilities of different molecules are often very different so that the strength of Rayleigh scattering can be used to infer the types of molecules or atoms with which the light is interacting.

The intensity of Rayleigh scattering is often described by defining an angular cross section for each individual molecule, σ, as the scattered power per unit solid angle (intensity) divided by the incident power per unit area (irradiance). For a gas of number density N consisting of isotropic molecules (all of the elements of the diagonalized polarizability tensor are equal) the angular cross section is related to the index of refraction by

$$\sigma^{i}(90^{o}) = 4\pi^{2}(n - 1)^{2}/(N^{2}\lambda^{4}) \qquad (2.1)$$

where the superscript i refers to an isotropic molecule, n is the index of refraction of the gas, and λ is the wavelength of the light. This expression is derived for an ideal gas assuming $n - 1 \ll 1$.

The intensity of Rayleigh scattering from a unit volume of pure gas at a constant temperature is directly proportional to the number density of the gas and the irradiance of the incident light source. The polarization of the

scattered radiation can be characterized by defining $I_{\parallel}$ as the intensity of scattered light polarized parallel to the electric field of the incident light and $I_{\perp}$ as the intensity polarized perpendicular. For an isotropic molecule these relationships give

$$I_{\parallel}^{i}(90^{o}) = \sigma^{i}(90^{o})NI_{o} \tag{2.2}$$

$$I_{\perp}^{i}(90^{o}) = 0 \tag{2.3}$$

where I_o is the incident laser light irradiance and N is the number density of the gas.

For anisotropic molecules at least two of the diagonalized elements of the polarizability tensor are not equal, and an incident radiation field will induce a dipole moment within the molecule which is, in general, not parallel to the electric field of the radiation. In this case $I_{\perp} \neq 0$. The effects of molecular anisotropy are usually treated by defining the depolarization ratio

$$\rho = I_{\perp}/I_{\parallel} \tag{2.4}$$

and using scattering theory to show that Eq. (2.1) must be modified so that the anisotropic angular scattering cross section for linearly polarized light becomes

$$\sigma^{a}(90^{o}) = 4\pi^{2}(n - 1)^{2}\,(3/(3 - 4\rho))/(N^{2}\lambda^{4}) \tag{2.5}$$

Using Eq. (2.5) it can be shown that

$$I_{\parallel}^{a}(90^{o}) = \sigma^{a}(90^{o})NI_{o} \tag{2.6}$$

and

$$I_{\perp}^{a}(90^{o}) = \sigma^{a}(90^{o})N\rho I_{o} \tag{2.7}$$

Values of ρ for most molecules are small, but vary over a range from zero to as large as approximately 0.15.

Since the intensity of light scattered from individual molecules is additive, the total intensity of Rayleigh scattering from a mixture composed of M different gases can be written as

$$I_{\parallel}^{a}(90^{o}) = N\left(\sum_{j=1}^{M} \sigma_{j}^{a}(90^{o})X_{j}\right) I_{o} \tag{2.8}$$

$$I_{\perp}^{a}(90^{o}) = N\left(\sum_{j=1}^{M} \sigma_{j}^{a}(90^{o})\rho_{j}X_{j}\right) I_{o} \tag{2.9}$$

where X_j is the mole fraction of gas j and N is the total number density, $N = \sum_{j=1}^{M} N_j$, of the mixture. By using Eqs. (2.8) and (2.9) along with the condition $\sum_{j=1}^{M} X_j = 1$, the mole fraction of each component in an isothermal mixture of three gases can be determined by measurements of $I_{\parallel}^{a}(90^{o})$ and $I_{\perp}^{a}(90^{o})$ providing each gas has different values of σ_j and ρ_j. However, if there are more than three gases in the mixture or if the values of σ_j and ρ_j are not different for each gas, the system will be underdetermined and it will be impossible to solve for individual X_j.

When the system is not isothermal the total number density of a constant pressure gas mixture is inversely proportional to temperature. In this case, Eqs. (2.8) and (2.9) can be rewritten as

$$I_{\parallel}^{a}(90^{o}) = N_{o}(P/RT)\left(\sum_{j=1}^{M} \sigma_{j}^{a}(90^{o})X_{j}\right) I_{o} \qquad (2.10)$$

$$I_{\perp}^{a}(90^{o}) = N_{o}(P/RT)\left(\sum_{j=1}^{M} \sigma_{j}^{a}(90^{o})\rho_{j}X_{j}\right) I_{o} \qquad (2.11)$$

where N_o = Avogadro's number = 6.023×10^{23}, P is the total pressure, R is the gas constant, and T is temperature. Providing the values of σ_j and ρ_j are different for each gas and independent of temperature, the maximum number of properties which can be uniquely determined are the temperature and the mole fractions of two gases. It should be mentioned that the radiation scattered by gas molecules is spectrally broadened due to molecular translational motion (Doppler broadening). An evaluation of the spectral broadening of Rayleigh scattered light can be used to derive a temperature in a turbulent flow measurement as shown by Robben [26].

2.2 Past Uses of Rayleigh Scattering as a Probe in Turbulent Flow Systems

Several groups have used Rayleigh scattering as a probe of scalar fields in turbulent combustion. Since a combustion system contains more than two gases, the actual quantity measured depends on the conditions of the experiment and assumptions (expected to be very good) must be made to obtain meaningful results and overcome the nonspecificity of this type of scattering. Robben [26] has argued that the contribution of each atom to Rayleigh scattering is relatively independent of how it is bonded. This implies that for a premixed combustion system the total Rayleigh cross section is independent of the degree of reaction and therefore the scattering intensity will be proportional to the mass density within the observation volume. If the total number of molecules in the flow does not change significantly as a function of

the degree of reaction, the mass density will be proportional to the number density of the gas. This criterion is found to be nearly true for many combustion systems and Rayleigh scattering has been used to measure number density for a variety of turbulent combustion configurations [27-32].

If the pressure of the combustion system is constant (an open system) and the assumption is made that the gas is ideal, the number density is inversely proportional to temperature. This relation was used by Müller-Dethlefs and Weinberg [33] to measure temperatures in flame speed experiments. Dibble and coworkers [34-37] have used this method to measure temperature fluctuations in turbulent premixed flames and have also demonstrated that the technique can be extended to turbulent diffusion flames where the fuel and air have been carefully chosen to have identical Rayleigh scattering cross sections. These workers [38,39] have also demonstrated a technique in which Rayleigh scattering and laser anemometry are combined to determine density and velocity at essentially the same time and point in space. Pitz et al. [27] have used measurements of Doppler profiles to measure temperatures in a hydrogen-air flame.

Rayleigh scattering has also been used for monitoring the concentration fluctuations which occur in isothermal turbulent flows [1,2]. In these experiments, real-time concentration measurements were made for axisymmetric fuel jets issuing into a slow flow of surrounding air. As long as the scattering cross sections of the two gases are not the same, a single measurement of total Rayleigh scattering intensity allows a determination of the mole fractions of the two components. Equation (2.8) can be rewritten as

$$I(90^{o}) = (\sigma_a X_a + \sigma_f X_f)NI_o \qquad (2.12)$$

where σ_a and σ_f are the observed 90^{o} scattering cross sections for air and fuel, respectively. As long as the pressure and laser intensity remain constant, the only unknowns in the equation are X_a and X_f. The mass conservation equation

$$X_a + X_f = 1 \qquad (2.13)$$

provides the second relation necessary for the determination of X_a and X_f.

Graham et al. [1] were the first to report Rayleigh scattering measurements of this type. These workers studied the fluctuations which occur in acoustically forced and unforced jets of methane into air. This work demonstrated that Rayleigh scattering can be used to observe concentration fluctuations in a turbulent flow system. Later, Dyer [2] used the same technique to measure the average concentration and RMS concentration fluctuations as a function of position in a jet of propane. This work also included results of autocorrelation measurements which allowed the integral time scale (defined in Section 4.5) to be determined for known positions in the turbulent flow. Simple statistical arguments were provided indicating that measurements performed in this manner are very accurate.

2.3 Expected Signal and Noise Levels for Rayleigh Scattering Measurements

Equation (2.12) gives the intensity of light scattered in the perpendicular direction from a light source of known I_o. In order to relate this

equation to the signal measured in an experiment it is necessary to include the effects of the solid angle for the collection optics, optical losses, and detector efficiency. The following expressions are derived in terms of photons (or events)/s.

It is important to note that the output of the photomultiplier is a current and that this output may or may not consist of discrete detection events. For instance, at low light levels a discriminator/amplifier combination may be used to detect amplified photoelectron pulses arriving at the anode of the photomultiplier and counters can be used to relate the number of detected photons to the light intensity. This photon counting technique is highly compatible with digital data acquisition. However, at high light intensities the number of detected photons becomes very large and electronic detection devices can no longer distinguish individual events. This pulse "pile-up" leads to nonlinearities in the ratio of detected current pulses to the actual number of photons reaching the anode of the photomultiplier. In this case, it is preferable to measure the total current output of the photomultiplier. If the gain (G) of the photomultiplier is known, the number of detected photons (N_P) during a time period (Δt) is related to the current (i) by the relation

$$N_P = \int_o^t i dt/(G \times 1.6 \times 10^{-19}) \qquad (2.14)$$

where i has units of amps and the integral represents the total charge collected during Δt.

The following equation gives the predicted photon detection rate during a laser Rayleigh scattering experiment when the laser is assumed to have a cylindrical profile within the observation volume of the collection optics.

$$R_P = I_L \eta_L l \Omega \eta_C \varepsilon N \sum_{j=1}^{M} \sigma_j X_j \qquad (2.15)$$

where

R_P = detected photoelectron rate (photons/s)

I_L = laser output (photons/s)

η_L = coefficient of optical transmission between the laser and observation volume

l = length of observed volume element

Ω = solid angle (steradians) of collection for scattered light

η_C = coefficient of optical transmission between observation volume and detector

ε = quantum yield of photomultiplier

$N \sum_{j=1}^{M} \sigma_j X_j$ = Rayleigh scattering cross section for gas of total number density N

This equation is based on several assumptions including 1) observations are made at right angles to the laser beam, 2) polarization effects are absent, and 3) Ω is small enough to avoid considering the angular dependence of Rayleigh scattering.

In order to obtain an estimate of the number of photons which should be detected in an actual experiment, R_p has been calculated assuming that scattering is induced from air by a 7 watt argon ion laser operating at 488 nm. The following parameters have been chosen to approximate those actually existing in our experimental system.

$$I_L = 1.72 \times 10^{19} \text{ photons/s}$$

$$\eta_L = 0.67$$

$$l = 0.027 \text{ cm}$$

$$\Omega = 0.189 \text{ sr (f/2 collection optics)}$$

$$\eta_C = 0.50$$

$$\varepsilon = 0.14$$

$$N = 2.46 \times 10^{19} \text{ cm}^{-3}$$

$$\sum_{j=1}^{M} \sigma_j X_j = \sigma_{AIR} = 8.2 \times 10^{-28} \text{ cm}^2/\text{sr}$$

Using these parameters, the detection rate of photons is calculated to be $R_p = 8.3 \times 10^7$ photons/s.

The use of Rayleigh scattering as a concentration probe requires an estimate of the accuracy with which a measurement of a given scattering intensity can be made during a time period Δt. Much of the material which follows is described in detail by Robben [40] in his paper on noise in the

measurement of light with photomultipliers. The detection of photons obeys Poisson statistics, which require that a repeated measurement of the number of detected photons, N_p, from a constant intensity light source during Δt will have a variance equal to the average number of photons detected during Δt. This requirement is expressed as

$$\mathrm{Var}(N_p) = \langle N_p \rangle \tag{2.16}$$

where $\langle N_p \rangle = \lim_{L \to \infty} \sum_{j=1}^{L} \frac{(N_p)_j}{L}$. The relative uncertainty in a measurement of N_p is given by

$$\mathrm{Var}(N_p)^{1/2} / \langle N_p \rangle = 1/\langle N_p \rangle^{1/2} = 1/\langle R_p \Delta t \rangle^{1/2} \tag{2.17}$$

The uncertainty in optical measurements due to Poisson statistics is sometimes called electronic shot noise. Equation (2.17) shows that in order to reduce the relative uncertainty in the measurement of a Rayleigh scattering intensity it is necessary to lengthen the counting period or to increase R_p by increasing the intensity of light reaching the detector.

An estimate of the relative uncertainty in the intensity measurement of Rayleigh scattering from air for the conditions described above can be obtained by the use of Eq. (2.17). For a one second counting time the predicted relative uncertainty is only 0.00011. However, for a one microsecond counting time the relative uncertainty is 0.11. Clearly, the minimum time resolution which can be obtained with Rayleigh light scattering concentration measurements depends on the maximum relative uncertainty which is tolerable in the experimental measurement.

When analog detection of the photomultiplier current output is used, Eq. (2.17) is modified by combining it with Eq. (2.14) to give

$$\mathrm{Var}(q_t)^{1/2}/\langle q_t\rangle = ((G \times 1.6 \times 10^{-19})/\langle q_t\rangle)^{1/2} \qquad (2.18)$$

where $q_t = \int_o^t i\,dt'$. Equation (2.18) describes the relative uncertainty in the intensity measurement assuming no additional uncertainty is introduced by the amplification which occurs along the dynode chain following the release of a photoelectron at the photocathode of the photomultiplier. In practice, the amplification of current at each dynode in the chain also obeys Poisson statistics and an extra term must be included in Eq. (2.18) to represent this source of noise.

$$\mathrm{Var}(q_t)^{1/2}/\langle q_t\rangle = ((\alpha/(\alpha - 1))(G \times 1.6 \times 10^{-19})/\langle q_t\rangle)^{1/2} \qquad (2.19)$$

α is the gain per dynode within the photomultiplier and a large number of dynodes has been assumed. A typical value of α is 5, so the relative noise is increased by ~1.12 over what it would have been in the absence of amplification noise. Equation (2.19) is for the case where the current from the photomultiplier is integrated for a period Δt. Often, the current outputs of photomultipliers are not integrated for a given time period, but are instead "smoothed" by RC time constant circuits or cut-off frequency filters. In these cases the integration period must be replaced with an effective time period, $\Delta t'$, which is related to the cut-off frequency by the expression $\Delta t' = 1/(2\Delta f)$ where Δf is the frequency bandpass of the filter. Equation (2.19) can be rewritten as

$$\mathrm{Var}(q_t')^{1/2}/\langle q_t' \rangle = ((\alpha/(\alpha - 1))(G \times 1.6 \times 10^{-19})/\langle q_t' \rangle)^{1/2} \qquad (2.20)$$

where $q_t' = i_{AVG}\,\Delta t'$ and i_{AVG} is the average current during $\Delta t'$.

The equations discussed thus far only predict the observed variation in numbers of detected photons for light from a constant intensity source. In cases where the light intensity is varying, these equations are no longer strictly valid. However, for moderate numbers of photocounts, it is found that the relative error in a single measurement of the integrated light intensity during a time period Δt is essentially equal to Eqs. (2.17) or (2.20) where $\langle R_P \Delta t \rangle$ and $\langle q_t' \rangle$ are replaced by $R_P \Delta t$ and q_t', respectively.

There are often other sources of noise in scattering measurements which can interfere with accurate determinations of Rayleigh scattering intensity, such as source fluctuations, dark current, and background interference. Becker et al. [15] and Shaughnessy and Morton [16] have given detailed discussions of such sources of noise in regards to scattering from particles (Mie scattering). Similar considerations are expected to be important for scattering from molecules. For the experiments reported here, we conclude that electronic shot noise is by far the largest noise factor and that other noise sources can be disregarded.

For the experiments described here, Rayleigh scattering is used to produce a time record of concentration fluctuations occurring in a turbulent flow of fuel (methane) into a slow flow of air. The light which is detected by the photomultiplier consists of scattering from the molecules within the flow and background radiation from light scattered by the apparatus and other

sources. It is therefore necessary to deconvolute the scattering due to actual Rayleigh scattering from background light. We have used a calibration procedure in which scattering from air and methane are measured before the turbulent flow of methane into air is initiated. These intensities are recorded for a relatively long time to ensure that the errors in the measurements are small. The intensity of scattering from the turbulent flow is then recorded in an identical manner. The mole fraction of methane is then obtained directly from the relation

$$X'_{CH_4} = (I_{tur} - I_{AIR})/(I_{CH_4} - I_{AIR}) \tag{2.21}$$

where I_{tur}, I_{AIR}, and I_{CH_4} refer to Rayleigh scattering intensities from the turbulent flow, air, and methane, respectively. This equation can easily be obtained from Eq. (2.12). Note that each intensity contains contributions from background radiation, but that the background contribution drops out when the differences in Eq. (2.21) are taken. The value of each X'_{CH_4} will have an error due to electronic shot noise in the measurement of I_{tur}. Fortunately, methods exist for statistically compensating for electronic shot noise when calculating many of the quantities of interest for the turbulent flow. These techniques are considered in the following section.

3. TURBULENCE MEASUREMENTS

3.1 Nature of Turbulence and Approaches to Its Characterization

In early experimental studies of turbulence most investigators were primarily concerned with averaged measurements of turbulent quantities. This

was due to the widely held belief that turbulent flow was very close to being a totally random phenomenon and that the only hope for treating it was by the use of statistical techniques. Such a viewpoint is inherent in the use of the Reynolds decomposition of the Navier-Stokes equations. A primary hypothesis of this approach is that turbulence consists of a wide size range of eddies which are randomly distributed in space and time and that there is a constant cascade of turbulent energy from larger to smaller eddies. In order to characterize this structure, such measurements as averages, standard deviations (turbulent intensity), and power spectra were made for the velocity fluctuations within turbulent flow fields.

Recently this focus has begun to change. Studies such as that of Brown and Roshko [41] have found that turbulent flows have a highly organized large scale structure. This has led to a resurgence in the use of visualization techniques to characterize these structures. The existence of these organized large scale structures has also increased the need for such measurements as intermittency and conditionally sampled statistical measurements which require time-resolved techniques.

Most past experimental studies have dealt with velocity measurements within the turbulent flow field. Measurements of scalar quantities such as temperature and concentration have lagged far behind. The preponderance of measurements of velocity flow fields is due to the importance of momentum transfer in theories of turbulence and the availability of sensitive techniques for velocity determination. Accurate methods for scalar quantities are much less developed than those for velocity. It should be noted that the transport of heat and mass within turbulent flows is one of the primary

reasons for their practical importance. Furthermore, any theory of turbulence based on velocity behavior should also be able to predict heat and mass transport in order to be complete. Clearly, accurate measurements of scalar flow fields are required.

3.2 Calculational Methods for Properties of the Concentration Flow Field

Our work uses Rayleigh light scattering as a probe of the time-resolved concentration fluctuations occurring in a turbulent flow. The raw data which are generated are digitized and stored in the memory of a minicomputer. This subsection describes how the data are analyzed in order to describe the properties of the concentration fluctuations at a point in space.

The first requirement is to characterize the statistical distribution of the concentration fluctuations. We have chosen to do this by use of the average concentration and the second through fourth central moments of the distribution. For a series of L noise-free concentration measurements (in mole fraction terms) the average concentration is given by

$$\bar{X} = \left(\sum_{j=1}^{L} X_j \right) / L \qquad (3.1)$$

where $\bar{X}$ is the average concentration and X_j is the result for a single measurement. The second and higher central moments of the concentration distribution are defined as

$$\mu_r = \left(\sum_{j=1}^{L} (X_j - \bar{X})^r \right) / L \qquad (3.2)$$

where μ_r is the rth central moment of the concentration distribution.

The second central moment is called the variance. Often the square root of the variance (called the standard deviation or root mean square (RMS)) is reported. In this work the RMS is denoted as $\tilde{X}$. The third and fourth central moments are often given in dimensionless terms by dividing them by a suitable power of the variance. The skewness factor is defined as

$$S = \mu_3/(\mu_2)^{3/2} \tag{3.3}$$

and the flatness factor or kurtosis as

$$K = \mu_4/(\mu_2)^2. \tag{3.4}$$

S and K can be considered as measures of how the experimental distribution differs from a Gaussian. For a perfect Gaussian S = 0 and K = 3.

In Section 2.3 it was pointed out that there is an electronic shot noise associated with every measurement of X'_{CH_4} using Eq. (2.21). This noise can lead to large errors in the calculated values of $\tilde{X}$, S, and K when it is comparable in size to the intensity changes in Rayleigh scattering due to concentration fluctuations. Fortunately, Birch et al. [23] have developed a very effective mathematical method for separating the actual moments of the intensity fluctuations (due to concentration fluctuations) from the effects of shot noise. These workers used the earlier results of Pike [42] who had shown that the moments of the photon number distribution are identical to the factorial moments of the detected photon distribution.

In order to apply the results of Pike [42], the detected Rayleigh scattering must be given as a series of numbers of detected photocounts, N_P, collected during a time period Δt. The factorial moments for the distribution of N_P are defined as

$$\left(\mu'_{(r)}\right)_{PC} = \left(\sum_{j=1}^{L} \left(N_P\right)_j^{(r)} \right)/L \tag{3.5}$$

where $\mu'_{(r)}$ is the rth factorial moment, the subscript PC indicates the photocount distribution, and $B^{(r)} = B(B-1)(B-2)\cdots[B-(r-1)]$ or $\frac{B!}{(B-r)!}$. According to Pike [42],

$$\left(\mu'_{(r)}\right)_{PC} = \left(\mu'_r\right)_{PF} \tag{3.6}$$

where $\left(\mu'_r\right)_{PF}$ are the moments of the photon field distribution. $\left(\mu'_1\right)_{PF}$ is the average number of photocounts during Δt and for scattering from a turbulent flow can be denoted $\bar{I}_{tur}$ and used in Eq. (2.21) to calculate $\bar{X}_{CH_4}$. In order to obtain the higher moments for the concentration distribution, the photon field moments must be converted to central moments using the relation

$$\left(\mu_r\right)_{PF} = \sum_{j=1}^{r} (-1)^j \binom{r}{j} \left(\mu'_{r-j}\right)_{PF} \left(\mu'_1\right)^j_{PF} \tag{3.7}$$

and then normalized to include only the scattering from gases in the field of view of the photomultiplier

$$\mu_r = \left(\mu_r\right)_{PF} / \left(I_{CH_4} - I_{AIR}\right) \tag{3.8}$$

where I_{CH_4} and I_{AIR} are the average numbers of photocounts defined earlier.

Power spectra are taken in order to determine the frequencies which compose the concentration fluctuations. For the case of a continuous function the power spectrum is defined as the square of the Fourier integral

$$\Phi(\omega) = \left| \int_{-\infty}^{\infty} X(t) e^{-i\omega t} dt \right|^2 \qquad (3.9)$$

where $\Phi(\omega)$ is the power spectrum. In our experiment, the Rayleigh scattering intensity is recorded at equally spaced times for a finite period of time. It can be shown that a very good approximation of $\Phi(\omega)$ can be calculated from discrete data if the highest frequency in the signal is no larger than one half of the sampling frequency (the Nyquist sampling theorem [43]) and the lowest frequency in the signal is sampled at least five times during the total data collection time. The calculated power spectrum does tend to be broadened and "noisy" due to digital effects arising from the incomplete transformation. A method known as the Fast Fourier Transform (FFT) due to Cooley and Tukey [44] is used to quickly calculate the Fourier transform for discrete data, and a simple complex multiplication then yields $\Phi(\omega)$. It should be noted that electronic shot noise is "white." This means that it is a constant intensity at all frequencies and a power spectrum due to concentration fluctuations measured by Rayleigh scattering will be built on a flat base due to shot noise.

A related function of interest is the correlation function, $R(\tau)$, defined as

$$R(\tau) = \int_{-\infty}^{\infty} X(t)X(t + \tau)dt \qquad (3.10)$$

$R(\tau)$ gives an indication of the time required for an average eddy to pass a point in space. In conjunction with Taylor's hypothesis [45], an average eddy size or length scale can be calculated if the velocity at the point is also known. The Fourier transform of the correlation function is the power spectrum

$$\Phi(\omega) = \int_{-\infty}^{\infty} R(\tau)e^{-i\omega\tau}d\tau \qquad (3.11)$$

thus either $\Phi(\omega)$ or $R(\tau)$ can be used to describe the period and frequency of concentration fluctuations and one is easily converted to the other. The minicomputer used in this study is programmed to calculate $R(\tau)$ by taking a FFT of $X(t)$, squaring the complex function which results, and taking the inverse Hermitian (reverse Fourier transform) of the square. The calculation of a correlation function from a discrete data set of finite length is subject to the same constraints as those for calculating Fourier transforms.

All of the functions describing the statistical behavior of the time dependent concentration fluctuations discussed thus far are averaged for the entire data set. However, it is well known that turbulent flows display a property known as intermittency (see Schon and Charnay [46] for a discussion) which is due to the presence of two distinct fluid behaviors in the instantaneous flow field. The regions where the fluid behavior varies are separated by a well defined boundary which is small compared to the size of the regions. The two types of fluid behavior have different statistical behaviors with regard to the property being measured which allow the location of the boundary between the two regions to be determined. These distinct regions of fluid behavior are thought to be due to the presence of large scale structure

in the turbulent flow field. In this work we are interested in the intermittency function, I(t), which describes the passage of the turbulent/nonturbulent boundary of the fluid through the observation volume. We have defined a turbulent region as existing when air has been entrained into the flow and a nonturbulent region as one where either only air or methane are present. The following equations can be written to mathematically describe this concept.

$$I(t) = 1 \text{ when } 0 < X_{CH_4}(t) < 1$$

$$I(t) = 0 \text{ when } X_{CH_4}(t) = 0,\ X_{CH_4}(t) = 1 \qquad (3.12)$$

This definition of turbulent intermittency based on concentration has been used by several research groups [16,47-49] and also in the similar case of heated flows where the marker is temperature [50]. By simultaneously monitoring temperature and velocity, Chevray and Tutu [51] demonstrated that the intermittency function derived by real-time monitoring of a temperature marker is identical to that found when velocity fluctuations are used.

Even though intermittency is a very simple idea conceptually, in practice is has proven very difficult to generate a concensus among workers in the field on an experimental definition. In part, this is due to the wide range of turbulence variables (e.g., velocity, vorticity, concentration) for which intermittency measurements have been made and the wide range of experimental techniques employed. In the case of velocity measurements the problem is severe since there is fluid motion in nonturbulent regions and it is necessary to base intermittency decisions on whether or not the velocity fluctuations

are characteristic of turbulent flow. This problem has led to detailed analysis and modeling in an attempt to overcome the problem [52,53]. For scalar quantities the problem is somewhat simplified since the decision is usually based on the presence or absence of the scalar (e.g., heat or mass). For these measurements, the accuracy of the determination of the interface location is usually limited by noise in the measurement of the scalar quantity. An additional difficulty arises due to the finite sampling volume of most probes. Fluctuations occurring in this volume are averaged and this can lead to inaccuracies in the determination of the boundary location. Many different approaches to solving or at least minimizing these problems have been used. In the experimental section (Section 4.5) we describe a procedure based purely on statistics and the noise level in the measurement.

Once an intermittency function is obtained it can be used to calculate several new properties of the flow field. The fraction of time the observation volume spends within the turbulent flow region is defined by the intermittency factor, γ, where

$$\gamma = \lim_{t\to\infty} \int_0^t I(t')dt'/t \qquad (3.13)$$

For discrete data an approximation of γ is calculated by summing the number of points at which I(t) = 1 and dividing by the total number of points. Clearly, the accuracy of γ will depend on the size of the eddies being observed and the length of time for which the measurement is made. This point will be discussed further in later sections. An intermittency frequency, symbolized f_γ, can be defined as the average number of times I(t) goes from 0 to 1 during a one second time period. It is obviously related to the number of large

scale structures passing through the observation volume. Unfortunately, values of f_γ have proven very difficult to reproduce among different laboratories. This observation is believed [54] to be due to the presence of very short bursts of turbulence in the observation volume which do not significantly modify the value of γ, but which modify the value of f_γ dramatically depending on whether or not they are detected.

Once an intermittency function is obtained, it is natural to use it to determine the statistical properties of the scalar field in the turbulent region only (by definition, the scalar quantity should be zero in the nonturbulent region). Such measurements are known as conditional sampling since the calculations are only performed when the condition $I(t) = 1$ is fulfilled. These conditionally sampled measurements are expected to be much more representative of turbulent behavior since they are made for turbulent fluid as opposed to the global measurements which are weighted by the presence of nonturbulent fluid. The average and moments of the turbulent concentration fluctuations can be obtained by rewriting Eqs. (3.1) and (3.2) as

$$(\bar{X})_T = (L\gamma)^{-1}\left(\sum_{j=1}^{L} X_j\, I(t)_j\right) \tag{3.14}$$

and

$$(\mu_r)_T = (L\gamma)^{-1}\left(\sum_{j=1}^{L} \left(X_j - (\bar{X})_{tur}\right)^r I(t)_j\right) \tag{3.15}$$

where $\mu_{r\ T}$ are calculated using Eqs. (3.5)-(3.8) when corrections must be made for electronic shot noise.

4. EQUIPMENT AND PROCEDURES

4.1 Flow System

The flow system used for this experiment consists of an axisymmetric jet of methane issuing into a slow flow of surrounding air. The jet is constructed from a 61 cm length of 6.35 mm I.D. brass tubing (9.5 mm O.D.). These dimensions ensure that fully developed pipe flow occurs in the tube before the methane exits the jet. The output end of the tube is sharpened to a fine edge and the upstream end is connected to a ballast chamber to minimize pressure fluctuations. Since Rayleigh scattering measurements are extremely sensitive to interference from particle (Mie) scattering, it is necessary to enclose the entire flow system to prevent dust particles from reaching the observation volume. For this reason the jet is centered inside a 10.4 x 10.4 x 61 cm enclosure constructed from 5 mm thick optical crown glass. A flow of air enters the enclosure from the bottom after passing through a bed of polystyrene balls and a wire gauze to ensure a homogeneous flow. Flows of both methane and air are controlled and measured by Fischer and Porter Flowrator meters.[2] Both flows are prefiltered with 0.3 micron filters to remove particles. Methane (Matheson Technical Grade, >98%) is obtained from a cylinder. A regulated, house-compressed air line is the source of air.

The initial stages of this work were plagued with scattering from particles and unexpected profiles for the concentration field of the methane

[2]Certain commercial equipment, instruments, or materials are identified in this paper in order to adequately specify the experimental procedure. Such identification does not imply recommendation or endorsement by the National Bureau of Standards, nor does it imply that the materials or equipment are necessarily the best available for the purpose.

jet. Subsequent analysis indicated that the source of the problem was recirculation within the enclosure. (See Becker et al. [47,55] for a good discussion of this behavior.) Recirculation occurs when the ability of the jet to entrain surrounding gas is greater than the amount of surrounding gas present. In this case gas is drawn from downstream and recirculation eddies develop. Since the entrainment rate of the jet is proportional to the Reynolds number (Re), the higher the flow rate the more likely the occurrence of recirculation. Becker et al. [55] analyzed the likelihood of recirculation in terms of the Craya-Curtet number Ct. Using their analysis it is possible to show that recirculation should occur for the initial flow conditions used in this study. In order to eliminate recirculation, it is necessary to reduce the difference in flow rates between the air and methane. When this is done recirculation effects disappear. The absence of such effects is confirmed by hot-wire velocity profiles which are found to be identical with or without the enclosure in place. All measurements reported here are for an initial methane flow velocity of 1022 cm/s and a surrounding air flow velocity of 26.9 cm/s. These velocities correspond to a Reynolds number of $Re = uD/\nu = 3760$ where u is the difference in initial velocities of the two flows, D is the diameter of the jet, and ν is the kinematic viscosity of methane.

The jet and enclosure are mounted on a lathe bed to allow accurate positioning of the observation volume in the flow field. Scales mounted on the lathe bed give positions of the observation volume relative to the center of the nozzle exit which are accurate to 0.25 mm.

4.2 Optical System

Figure 1 shows the optical system used in this study. A Spectra-Physics Model 171-19 Ar ion laser is operated in the single wavelength mode to produce a 7 watt output at 488 nm. The laser beam is expanded to 22 mm using a 10X beam expander from Special Optics and is then focused to a narrow cylinder of ~ 0.035 mm diameter within the system enclosure by a lens (fl = 25 cm). The position of this focus along the laser beam is determined by a knife edge test. The approximate length of the cylindrical region over which the focused laser beam diameter remains constant is 4 mm.

Light scattered from the observation volume is collected and collimated by an anti-reflection (AR) coated 10.2 cm achromatic lens (f/2) and then refocused using a 10.2 cm AR coated spherical lens. A set of adjustable slits is placed at the focal point of the second lens to define the observation length of the cylindrical region of scattering. The diameter of the volume is determined by the diameter of the laser beam. By using the laser to back-illuminate a 0.025 mm pinhole, it is possible to determine the actual length of the observation volume by translating the pinhole along the laser beam path. Figure 2 shows plots of observed intensity versus position along the laser beam path for slit widths of 0.2 mm and 0.4 mm. The slight asymmetry in the plots is believed to be due to a minor misalignment of the slits relative to the optic axis. The origin of the plots is the point of minimum diameter for the laser beam. For slit widths less than 0.2 mm the same curve was obtained as for 0.2 mm slits. If it were possible to focus the image of the pinhole on the slits without distortion, the image size would be 0.025 mm. Figure 2 shows that this is clearly not the case. Spherical aberration causes

the minimum optical resolution to be ~0.27 mm. This results from light collected at different angles by the collection optics being focused at different distances from the lens. In order to minimize the length of the observed volume it is necessary to very carefully position the slits at the minimum diameter of the focus. The cross section of the focused light where this minimum occurs is known as the circle of least confusion (see Hecht and Zajac [56]). As the slits are opened the effects of spherical aberration become much less noticeable and the observed cylindrical volume has a length which is nearly equal to the slit width. The minimum volume element which can be resolved using the current optical system is estimated to be 0.0003 mm^3.

After passing through the slits, the light is again collimated with a 22.5 mm AR coated lens. It is then filtered by a Promfret Research Optics narrow bandpass filter centered at 488 nm and having a 1.2 nm FWHM and maximum transmission of 60%. Finally, a second 22.5 mm lens is used to focus the scattered light on the photocathode of a photomultiplier tube.

4.3 Detection, Conditioning, and Recording Electronics

The EMI 9781B photomultiplier tube used in this study has a modified S-5 photocathode with a reported quantum efficiency of 0.14. In all experiments described here the tube was operated at 680 volts. The calibrated gain for this voltage is reported by the manufacturer as $G = 2.4 \times 10^6$.

The output of the photomultiplier is measured in the current mode. A variable resistor is used to convert the current into a voltage which is fed to an Ithaco Model 4302 dual filter employed as a low pass 10X amplifier.

This filter provides a relatively sharp cut-off frequency which attenuates frequencies higher than a preset value at 24 dB/octave. Input voltages are adjusted so that a suitable output voltage (<2 volts) is produced for signal acquisition. The time response of the electronics is such that the filter provides all frequency selection and smoothing of the photomultiplier signal.

After conditioning, the PM signal is fed to a 12 bit digitizer of a Nicolet 1180 data acquisition and processing system. This system is a minicomputer employing a 20 bit processor unit specially designed for laboratory use. It is equipped with a wide range of analog to digital (A to D) and digital to analog (D to A) converters. Our particular instrument has a 40 K memory and is interfaced to a Diablo Model 31 disk drive which allows 1,143,296 20 bit words to be stored on interchangeable disks. Communications to and from the machine are provided by a teletype, a paper tape reader, oscilloscope, and digital plotter. Manufacturer supplied software includes BASIC and FORTRAN compilers and general purpose programs for signal acquisition and analysis.

The digitizer of the minicomputer sequentially samples an input voltage at a user selected dwell time (3 μsec minimum). The actual digitization is done by the combination of a rapid sample and hold and a much slower A to D. The digitized input signal, which is proportional to the smoothed current output of the photomultiplier, is stored in memory. Data sets as large as 32 K can be recorded in a single scan. At the conclusion of a data collection cycle the entire data set is transferred to the disk for later analysis.

4.4 Experimental Procedures

We have chosen to measure the methane mole fraction using Eq. (2.21). This equation requires that only relative Rayleigh scattering intensities and not absolute quantities be measured. For each turbulence measurement it is necessary to measure the scattering intensity due to methane and air. Data records of 4096 points are taken for each gas. Software programs are available for rapidly calculating average intensities and standard deviations. Statistical analysis indicates that the relative error due to photon statistics in these average intensity measurements is much less than 1%. An additional measurement is made when the enclosure is filled with helium. Since the cross section for helium is only 0.015 of that for air, this intensity provides a good estimate of the background intensity from the enclosure in the absence of scattering gas. Due to the small size of the enclosure and the use of glass walls with 4% reflections at each air/glass interface, the amount of detected light which is not due to Rayleigh scattering is of the same order as the light scattered from air. This background light limits how close the observation volume can be placed to the nozzle because scattering of the background light from the nozzle is quite strong. By subtracting the background intensity from the intensities observed when air and methane are in the enclosure, the intensity ratio $I_{CH_4}/I_{AIR} = \sigma_{CH_4}/\sigma_{AIR}$ can be calculated. This ratio is used as a check to ensure that no systematic errors are being made in the measurements. An indication of the reproducibility of the measurements can be found in the average value of $\sigma_{CH_4}/\sigma_{AIR} = 2.33 \pm 0.02$ found for ten different data sets recorded on the same day. Actual values of σ_{CH_4} and σ_{AIR} for ambient conditions are calculated using Eq. (2.1) and values of n_{AIR} and n_{CH_4} at 488.

nm taken from tables in McCartney's book [25] and Landolt-Börstein [57], respectively. The results are $\sigma_{AIR} = 8.17 \times 10^{-28}$ cm^2/sr and $\sigma_{CH_4} = 1.91 \times 10^{-27}$ cm^2/sr giving a predicted value of 2.34 for $\sigma_{CH_4}/\sigma_{AIR}$. Agreement between observed and predicted values is excellent. As a final check of intensity calibrations, a second data set is recorded for air after the turbulence data have been taken. If the two intensities measured for air differ by more than 1%, the entire series of measurements is repeated.

Immediately after calibrating the Rayleigh scattering intensity, a turbulent flow of methane into air enters the enclosure. After allowing a sufficient period of time for the flow to flush the enclosure and to stabilize, the Rayleigh scattering intensity is measured. The size of the turbulent data record can be varied, but for the experiments reported here either 16,384 or 32,768 real-time intensity measurements were recorded and stored on disk.

4.5 Data Analysis

The properties of the concentration fluctuations discussed in Section 3.2 are calculated at different positions in the flow field. As previously noted, Rayleigh scattering intensities recorded in the memory of the computer are only relative values and contain errors due to photon statistics. In order to apply Eqs. (3.5)-(3.8) for the calculation of concentration moments it is necessary to know the actual numbers of photons detected. We have used Eq. (2.17) as a means of providing a calibration factor for changing the relative intensities into absolute numbers of detected photons. Measurements of scattering from air and methane provide relative light intensities for two

well defined methane concentrations. These measurements also yield the relative standard deviations. It is worthwhile to note that the ratio of the standard deviations for the two measurements is found, as expected, to be inversely proportional to the square root of the intensity ratio. By using the relative standard deviation for scattering from air and substituting in Eq. (2.17) it is possible to calculate an effective value for the number of photons detected during a period equal to the dwell time. This number provides the calibration factor necessary to scale all of the relative intensity measurements in the computer memory to numbers of detected photons. Software has been developed using Eqs. (3.1)-(3.8) to calculate the average, standard deviation, skewness, and kurtosis for the turbulent methane concentration time histories. During software development it was found that round-off errors severely affected factorial moments calculated using Eq. (3.5) due to the large magnitudes of the numbers involved. In order to reduce this error it is necessary to calculate central factorial moments using

$$\left(\mu_{(r)}\right)_{PC} = \left(\sum_{j=1}^{L} \left(N_{P_j} - \mu'_1 \right)^{(r)} \right) / L \qquad (4.1)$$

and convert these to factorial moments using

$$\left(\mu'_{(r)}\right) = \sum_{j=1}^{r} \binom{r}{j} \mu'_{(r-j)} \mu_1^{(j)} \qquad (4.2)$$

These calculations were found to be much less susceptible to round-off errors.

Power spectra of concentration fluctuation data are calculated by first using routines provided by Nicolet to take the fast Fourier transform and then applying a complex multiplication to give the power spectrum. Power spectra

of entire data sets give high frequency resolution, but result in a large amount of digital noise. For this reason, the data are broken into smaller data records of 1024 data points. Fourier transforms for each of these smaller records are averaged and a power spectrum taken of the average. Even though the resulting power spectrum has much less frequency resolution, the digital noise is greatly reduced. This method of calculating power spectra from digital data has often been applied before. (See Konrad [49] and Cheng et al. [29] for examples.)

Correlation functions for the turbulent concentration data records are calculated using a subroutine of Nicolet's general applications package. The entire data record of 16,384 or 32,768 measurements is treated in a single calculation. Every data set recorded in this study gave $R(\tau)$ functions which could be fit as exponentials. For this case, the Eulerian or integral time scale (T) can be written as

$$T = \int_o^\infty R(\tau)d\tau = \int_o^\infty e^{-\tau/T}d\tau \qquad (4.3)$$

which is simply equal to the time constant for the decay of the correlation function. A linear least squares fit is used to calculate T from the log of the correlation function.

A simple algorithm has been developed for making intermittency decisions. These decisions are complicated by the relatively large error in the individual measurements due to Poisson noise. Clearly, the ability to differentiate turbulent from nonturbulent fluid will depend on the noise level. As discussed above, this noise level is directly related to such

factors as averaging time (cut-off frequency), laser power, and observation volume. We have chosen to make intermittency decisions based purely on statistical grounds. The fluid is considered to have become turbulent when five "independent" intensity measurements fall above the sum of the scattering intensity for air and one half of the standard deviation in the air measurement. The number of data points required to equal five independent measurements is calculated by dividing 5 by the product of the dwell time and the cut-off frequency. Using the above criterion, the probability that the gas contains a measurable concentration of methane is 0.997. The gas is defined as having returned to nonturbulent behavior when the average of five independent measurements falls below the defined cut-off level. It should be noted that many other equally valid criteria could be selected to define intermittency. Even though this prescription for calculating the intermittency function is somewhat arbitrary, it does yield results which are in agreement with visual inspections of the data and which behave very much like those reported in the literature. Additionally, it does seem to give results which are fairly independent of the cut-off frequency used for the experiment.

Intermittency frequencies are calculated by determining the number of times the intermittency function changes from 0 to 1 during a data record and dividing by the total collection time for the data record.

Once the intermittency function is available, conditionally sampled quantities are calculated for the turbulent region. The average methane concentration, standard deviation, skewness, and kurtosis values for the turbulent fluid are calculated as described above for the entire data record.

All of the above discussion on concentration measurements has been in terms of volume (or mole) fractions. Often, the concentration fields of turbulent jets are given in terms of mass fraction concentrations (see Way and Libby [9] and Birch et al. [23] for examples) in an attempt to allow the comparison of jets with varying density. The use of mass fractions automatically corrects for differences in jet behavior due to momentum differences based on density. Birch et al. [23] have given the following approximate equations for converting mole fraction concentrations into mass fraction terms

$$\bar{Y}_{CH_4} = (\alpha_\rho + 1)\bar{X}_{CH_4} / \left(\alpha_\rho \bar{X}_{CH_4} + 1\right) \tag{4.4}$$

$$\tilde{Y}_{CH_4} = (\alpha_\rho + 1)\tilde{X}_{CH_4} / \left(\alpha_\rho \bar{X}_{CH_4} + 1\right) \tag{4.5}$$

where $\bar{Y}_{CH_4}$ is the average concentration of methane in mass fraction terms, $\tilde{Y}_{CH_4}$ is the RMS of the methane concentration fluctuations in mass fraction terms, and α_ρ is the ratio of densities between pure methane and pure air minus one $\left(\alpha_\rho = \rho_{CH_4}/\rho_{AIR} - 1\right)$. Birch et al. [23] have concluded that there are no measurable differences using mass or mole fractions for skewness, kurtosis, correlation functions, or power spectra.

5. RESULTS

5.1 Nature of Detected Rayleigh Scattering

The average current output of the photomultiplier for scattering from air is measured to be ~13 μamps of which ~55% is due to Rayleigh scattering from air with the remainder being due primarily to scattered light from the

enclosure. Using Eq. (2.14), this corresponds to a photon detection rate of 3.4×10^7 photons/s or 1.9×10^7 photons/s for the Rayleigh scattering. This experimental value can be compared with the predicted value of 8.3×10^7 photons/s calculated in Section 2.3. Even though the two values differ by a factor of 4.3, the agreement is considered satisfactory since many of the parameters substituted in Eq. (2.15) are based on best case estimates. Additionally, the gain of the photomultiplier may no longer be the same as originally determined by the manufacturer.

As Eq. (2.20) shows, the relative uncertainty in a current (intensity) measurement from a photomultiplier is expected to be proportional to the square root of the cut-off frequency. Measurements of the standard deviation in detected intensity for a constant intensity source sufficient to generate a current of 15 μamps were made for three cut-off frequencies. The relative errors are summarized in Table 1. In each case, the observed relative errors are ~40% higher than predicted by Eq. (2.20). Much better agreement would be found if the photomultiplier gain is higher than the value used. Interestingly, a higher gain also leads to significant improvement in the agreement between the observed and calculated current for Rayleigh scattering from air.

Using the above results, it is possible to estimate the error in an individual methane concentration measurement when the actual concentration is $X_{CH_4} = 0.5$. X_{CH_4} is assumed constant for a time period which is greater than two times the inverse of the cut-off frequency. Assuming the current detected for air is 13 μamp and for methane is 22.6 μamp with 5.9 μamp from background scattered light, the 50% mixture of methane would be expected to give a signal of 17.8 μamp with relative errors of 0.026, 0.016, and 0.010 for cut-off

frequencies of 5700, 2280, and 1140, respectively. Using these values, the uncertainties in the concentration measurement are calculated to be 4.8, 3.0 and 1.9% of full scale. In actual practice, these values are expected to vary slightly as a function of operating conditions and methane concentration, but they represent a good estimate of the accuracy of a single methane concentration measurement with the experimental parameters of our experiment.

Figure 3 shows three 200 ms recordings of data at the same location in a turbulent flow of methane into air. These plots are uncorrected for photon statistics. The only parameter changed from one set of data to the next is the cut-off frequency of the amplifier which has values of a) 5700, b) 2850, and c) 1140 Hz. Also included in Fig. 3 are the expected uncertainties in each concentration measurement based on photon statistics which are extrapolated from measurements of scattering from air. Fluctuations due to turbulent concentration changes are clearly visible in each plot, but as the cut-off frequency is decreased the uncertainty in each individual measurement is visibly reduced. Significantly, when Eq. (3.8) is used to calculate the RMS, skewness, and kurtosis for the concentration fluctuations, the results for each of the three 32 K point data sets are in close agreement. This result indicates that the effects of fluctuations due to electronic shot noise can be deconvoluted from the time-averaged properties of the concentration distribution.

5.2 Time Averaged Properties of the Methane Concentration Field

Our goal in this work is to demonstrate the effectiveness of Rayleigh scattering as a concentration probe in isothermal turbulent flows involving

two different gases. As part of this study it is necessary to compare measured values of time-averaged concentration field properties with similar measurements made by other workers using different techniques and with the two past studies using Rayleigh scattering as a probe. For this reason, we have mapped out the centerline behavior as a function of the axial downstream distance (z) from the nozzle and the radial behavior (in terms of the distance r from the centerline) of the jet for one downstream distance (z = 111 mm).

Figure 4 shows a plot of reciprocal methane concentration versus axial distance which has been nondimensionalized by dividing z by the nozzle radius r_o. Note that the concentration of methane is given in both mole fraction, $\bar{X}_{CH_4}$, and mass fraction, $\bar{Y}_{CH_4}$, terms. The straight lines drawn through the data points are the results of linear least squares curve fits of the data for $z/r_o > 20$. To facilitate later comparisons, the dependence of mole fraction concentration on downstream distance is expressed in the form

$$\left(\bar{X}_{CH_4}\right)_o / \left(\bar{X}_{CH_4}\right)_c = C_1^X \left(z - z_o^{1X}\right)/r_o \qquad (5.1)$$

where $\left(\bar{X}_{CH_4}\right)_o$ is the concentration of methane at the nozzle exit $\left(\left(\bar{X}_{CH_4}\right)_o = 1\right)$, the subscript c indicates measurements on the jet centerline, C_1^X is a constant, and z_o^{1X} is the virtual origin in mole fraction terms. A similar equation is used for the mass fraction results

$$\left(\bar{Y}_{CH_4}\right)_o / \left(\bar{Y}_{CH_4}\right)_c = C_1^Y \left(z - z_o^{1Y}\right)/r_\varepsilon \qquad (5.2)$$

where $r_\varepsilon = r_o\left(\rho_{CH_4}/\rho_{AIR}\right)$ is an effective radius used by Birch et al. [23] in an effort to account for density differences between the methane and air.

This concept was originally introduced by Thring and Newby [58] and does seem to provide a good correction for density effects due to differences in temperature (see Wilson and Danckwerts [59]). C_1^X is found to equal 0.083 with $z_o^{1X} = -7.5\ r_o$, the fit of Eq. (5.2) gives $C_1^Y = 0.112$ with $z_o^{1Y} = -2.0\ r_o$.

Values of the RMS concentration fluctuations as a function of axial distance are shown in Fig. 5 for both mole and mass fraction representations. These data also seem to fall on straight lines. The two sets of data are fit to equations of the same form as Eqs. (5.1) and (5.2), namely

$$\left(\bar{X}_{CH_4}\right)_o / \left(\tilde{X}_{CH_4}\right)_c = C_2^X \left(z - z_o^{2X}\right)/r_o \qquad (5.3)$$

and

$$\left(\bar{Y}_{CH_4}\right)_o / \left(\tilde{Y}_{CH_4}\right)_c = C_2^Y \left(z - z_o^{2Y}\right)/r_o \qquad (5.4)$$

The data shown in Fig. 5 gives $C_2^X = 0.286$ with $z_o^{2X} = -34.8\ r_o$ and $C_2^Y = 0.569$ with $z_o^{2Y} = -11.9\ r_o$.

Often the behavior of RMS turbulent fluctuations is described in terms of fluctuation intensities. Concentration fluctuation intensity is defined as the local RMS of the concentration fluctuation divided by the local average concentration, $\tilde{X}_{CH_4}/\bar{X}_{CH_4}$ or $\tilde{Y}_{CH_4}/\bar{Y}_{CH_4}$. Concentration fluctuation intensity is often called unmixedness. Figure 6 shows the concentration fluctuation intensity along the jet centerline in both mole and mass fractions terms.

The behaviors of the skewness and kurtosis factors as a function of z are shown in Figs. 7 and 8, respectively. Even though there are fairly large

errors in the individual measurements, several distinct trends are evident in these results. The skewness is less than zero over the entire range of z values investigated. The skewness seems to reach a minimum at $z/r_o \approx 20$ and then gradually increases. Similarly, kurtosis values reach a maximum of ~3.8 near $z/r_o \approx 20$ and then fall to values in the 3 - 3.2 range as z increases. Note that both measures indicate a non-Gaussian distribution for the turbulent concentration fluctuations along the centerline of an axisymmetric jet.

Autocorrelation functions and power spectra have been calculated for all measurements taken along the jet centerline. Figure 9 shows examples of these functions for three values of z. Note that the frequency spectra are plotted as a function of log(relative spectral density) versus log(frequency). All of these spectra are taken from data recorded with a 4.6 kHz cut-off frequency. This cut-off frequency appears as a sharp dip in spectral density at high frequency values. For small values of z (z = 20 mm, $z/r_o = 6.3$) there is still some spectral density due to turbulent fluctuations at the point where the signal is attenuated by the filter. Clearly, some spectral information will be lost. By the time the flow is monitored at moderate downstream distances (z = 80 mm, $z/r_o = 25.2$) the high frequency portion of the spectral density due to concentration fluctuations is greatly reduced. A plateau in the spectral density is evident before the sharp drop due to the filter. This plateau is the baseline due to the white noise associated with photon detection statistics. This trend is much more evident further downstream (z = 159 mm, $z/r_o = 50.1$) where a wide plateau region is observed. The same power spectrum also shows a spike at 120 Hz which is an artifact due to a small frequency oscillation of the laser power. The spike is only observed at large values of z where the total fluctuation intensity is becoming weaker.

Integral time scales have been calculated from the autocorrelation functions using Eq. (4.3). Figure 10 shows the behavior of these time scales as a function of z/r_o. The time scales clearly increase with downstream distance, but due to the large variations between measurements it is impossible to give the form of the dependence. Birch et al. [23] have shown that the time scales should increase as the square of the downstream distance. We attribute the large variations in measured integral time scales to digital noise which results when the autocorrelation is taken for discrete data recorded over a relatively short period of time. The digital noise appears as random fluctuations which result in errors for the exponential fit to the decay of the function. These fluctuations can be clearly seen in the autocorrelations shown in Fig. 9.

All of the measurements reported above are for r = 0. We have performed similar measurements for the radial behavior of the concentration field at $z/r_o = 35$. Figure 11 shows the average methane concentration as a function of r (normalized by $r_{1/2}$, the radial distance at which the concentration has decreased to one half of its centerline value). Both mole and mass fraction concentrations are included. The solid lines are Gaussian-type functions of the form

$$\bar{X}_{CH_4} / \left(\bar{X}_{CH_4}\right)_c = \exp\left(-0.693(r/r_{1/2})^2\right) \qquad (5.5)$$

where the only independent variables are the centerline concentration and $r_{1/2}$. Values of these two parameters are taken directly from the data. These curves are in excellent agreement with both sets of data shown in the figure. Note that the values of $r_{1/2}$ used to fit the experimental values in

Fig. 11 differ slightly. For mole fraction concentrations $r_{1/2}/z = 0.108$ while the mass fraction results give $r_{1/2}/z = 0.104$.

The RMS concentration fluctuations normalized by the centerline value are shown in Fig. 12 in terms of mole and mass fractions. The solid line represents the results of Becker et al. [48] for an air-air axisymmetric jet and the dashed line gives the results of Birch et al. [23] in terms of mass fraction for a methane-air jet. Note that the turbulent intensity initially increases as a function of r. $\tilde{X}_{CH_4}/\left(\tilde{X}_{CH_4}\right)_c$ reaches a maximum of 1.31 at $r/r_{1/2} = 0.9$ while the RMS concentration in terms of mass fraction only reaches a maximum of 1.18 at $r/r_{1/2} = 0.7$.

Figures 13 and 14 show plots of the skewness and flatness factors for the methane concentration fluctuations as a function of $r/r_{1/2}$. Consistent with results in Fig. 7, the skewness on the jet centerline has a small negative value (~ -0.4), but as the measurement volume is moved outward in the radial direction the values of skewness continuously increase until near the edge of the jet they reach values greater than 5. As Fig. 14 reveals, the kurtosis value on the jet centerline is greater than the Gaussian value of 3. Initially, decreasing values of kurtosis are observed as the value of r is increased. This trend continues until the kurtosis has dropped to a value of ~2.5 at $r/r_{1/2} = 0.9$. After this minimum there is a rapid rise in kurtosis value and near the outer wings of the jet values in excess of 30 are observed. These two figures also include the results for conditional measurements which are described in the next section.

Power spectra and autocorrelation functions have been calculated for the radial measurements. The behavior of the integral time scales is shown in Fig. 15. Near the jet centerline the autocorrelation time is 1.5 ms, but as the measurement volume is moved outward from the centerline of the jet, a monotonic increase occurs and the integral time scale increases to values greater than 10 ms in the outer region of the jet. It should be noted that the signal to noise ratio is greatly reduced for the autocorrelation function as the edge of the jet is approached. This is due to the fact that only air is being monitored for a large fraction of the time. In these regions, fluctuations are only due to photon statistics, and since these are random they are uncorrelated and contribute a noisy zero baseline for the autocorrelation of the methane concentration fluctuations which occur during the fraction of time the fluid is turbulent.

5.3 Conditional Measurements in the Methane Concentration Field

All of the calculations discussed thus far are for total data records. However, as discussed in Section 3.2, the fluid in the outer regions of the jet displays an effect known as intermittency which results in two distinct types of fluid passing through the measurement volume element. The effect of intermittency is clearly seen in Fig. 16 where the methane concentration as a function of time is recorded for $z/r_o = 35$ and $r/r_{1/2} = 1.25$. During part of the sweep the methane concentration is zero while distinct "bursts" of mixed fluid can be observed at other times. It should be noted that these bursts appear to result in sharp increases of methane concentration when they enter the measurement volume and that the methane concentration then seems to die away slowly until nonturbulent fluid is once again present. As discussed

later, similar structures have been observed for the passive transport of heat in air-air jets.

The intermittency function calculated for the displayed portion of time-dependent methane concentration is also included in Fig. 16. Comparison of the observed methane concentration with the intermittency function shows that the algorithm described in Section 4.5 for intermittency determination gives a function which is in good visual agreement with the actual data. However, this figure also shows that very short bursts of turbulence (marked by arrows in the figure) are missed due to the averaging process inherent in the intermittency determination. It is found that most of the turbulent bursts are of relatively long duration and therefore we feel that the calculated intermittency functions are good representations of the actual behavior of the flow.

The intermittency factor, γ, has been calculated as a function of $r/r_{1/2}$ and the results are shown in Fig. 17 along with the corresponding intermittency frequency, f_γ. The measurements are based on concentration in terms of mole fractions. These results are not expected to be very different for mass fraction concentrations. It should be noted that values of f_γ are low and that they are subject to very large statistical error due to the few large scale structures which passed through the observation volume during the 3.3 s data collection time. This is especially true in the regions of very high or very low γ. The same argument indicates that measurements of γ will have large uncertainties in these regions also.

Several parameters can be defined which serve to characterize the behavior of the intermittency function. For instance, the value of the normalized radial distance where $\gamma = 0.5$ is found to be $r/r_{1/2} = 1.6$. Within the accuracy of the experiment the maximum of f_γ also occurs at $r/r_{1/2} = 1.6$. Previous workers have found that when values of γ determined from the transport of passive markers are plotted versus $r/r_{1/2}$ on probability graphs, linear curves are found. Figure 18 shows such a plot for the values of γ which are included in Fig. 17. This plot is found to be linear for all values of γ except those where round-off errors in the measurements become significant. The linearity of this plot requires that the location of the outer boundary of the jet be purely random. An equation can be written to describe the behavior of γ in terms of the average radial location of the jet edge ($\bar{R} = r$ where $\gamma = 0.5$) and the RMS value for the movement of the jet edge relative to this value, $\sigma_w = ((R - \bar{R})^2)^{1/2}$ [48]. σ_w is sometimes called the "wrinkle amplitude." Using these definitions, the following equation can be written to describe the r dependence of γ

$$\gamma = 0.5 \operatorname{erfc}((r - \bar{R})/\sqrt{2}\,\sigma_w) \qquad (5.6)$$

An analysis of the straight line in Fig. 18 gives $\bar{R} = 1.6\, r_{1/2}$ and $\sigma_w = 0.28\, r_{1/2}$. A plot of Eq. (5.6) is included in Fig. 17 and the agreement with experiment is very good.

Using intermittency functions such as that shown in Fig. 16, it is possible to calculate the average and higher central moments for concentration fluctuations in the turbulent ($I(t) = 1$) regions. These calculations are performed in terms of mole fraction concentrations. The general behavior is

expected to be the same if mass fraction concentrations are used. Figure 19 shows plots of $\bar{X}_{CH_4}$ and $\tilde{X}_{CH_4}/\left(\tilde{X}_{CH_4}\right)_c$ versus normalized radial distance along with the corresponding conditionally averaged quantities $\left(\bar{X}_{CH_4}\right)_T$ and $\left(\tilde{X}_{CH_4}\right)_T/\left(\tilde{X}_{CH_4}\right)_c$. As would be predicted, the average methane concentration is higher in the turbulent fluid than for the non-conditioned average. The concentration in the turbulent bulges decreases much more slowly than the overall average concentration with radial distance. The conditionally sampled RMS fluctuations as a function of normalized radius are decreased compared to the unconditioned results when γ is close to 1. However, as the value of γ decreases there is a crossover point at $r/r_{1/2} = 1.6$ for which $\left(\tilde{X}_{CH_4}\right)_T / \tilde{X}_{CH_4}$ is greater than 1.

The behaviors of conditionally sampled measurements of skewness and kurtosis are included in Figs. 13 and 14. The differences between conditionally sampled and overall measurements are striking at large values of r. This is not surprising, since in this region the fluid is 100% air for a relatively large fraction of the time and the lower end of the resulting methane concentration distribution must be cut off at this point. Conditional measurements indicate that while the skewness is still greater than zero and the kurtosis is greater than three in the turbulent regions, these parameters are constant or changing very slowly as a function of r.

6. DISCUSSION

6.1 Comparisons of Measurements from this Study with Other Work

The primary goal of this study has been the demonstration of a new technique for performing spatially- and time-resolved measurements in turbulent flows. In the course of this work a large amount of data has been generated which can be analyzed and compared with other work published in the literature. At the same time, we are confirming some past observations and reporting some new details of the behavior of the concentration field of an axisymmetric jet. In most cases, comparisons are made with results for similar jets of air issuing into air where the concentration field is not mapped directly, but either heat (small temperature differences) or small particles are assumed to have been passive markers for concentration fluctuations. There is one detailed study [23] where Raman scattering has been used to map out the concentration field behavior for a free axisymmetric jet of methane. Raman scattering is not sensitive enough to allow actual time-resolved measurements such as the intermittency and conditionally averaged flow parameters reported here. However, by clever analysis of their data, the authors were able to obtain accurate averaged properties for the concentration field. Santoro et al. [60] have used the promising new technique of optical tomography to measure the average concentration radial profile of a 10% methane in air jet. The results reported in this work are in very good agreement with all of these past studies, despite the fact that many of the parameters which might be expected to affect turbulent behavior (e.g., Reynolds number and initial flow conditions) vary in the different studies. The following section (Section 6.2) includes further discussion of this point.

Equations (5.1) and (5.2) can be used to compare results of Rayleigh scattering centerline concentration measurements with those found in other studies. Table 2 compares values of C_1^X, z_o^{1X}, C_1^Y, and z_o^{1Y} measured in this work with past measurements for air-air, methane-air, and propane-air axisymmetric jets. The data for propane jets is calculated for only the three sets of axial data reported by Dyer [2]. C_1^X and z_o^{1X} for the data of Birch *et al.* [23] are derived from results shown in Fig. 5 of their paper. There is no obvious relationship between the virtual origins of any of the measurements summarized in Table 2, but it is interesting that all of the other studies report positive virtual origins while this work gives negative values. Bradshaw [61] has argued that such differences are expected and depend on initial flow conditions. The most significant comparison of our results for centerline concentration behavior should be with the work of Birch *et al.* [23] who also studied a methane-air jet. Comparison of C_1^Y values listed in Table 2 shows that our value is ~10% smaller than the value found in the earlier work. However, these workers noted that the value of C_1^Y varies as the region of z/r_o for which it is determined is changed. They speculated that this is due to a slow approach to similarity (where similarity is used here to mean that the downstream behavior of the centerline concentration can be specified simply by the reduced variable z/r_o). These workers found that a determination of C_1^Y over the same region of z/r_o used in this work gave a value of 0.106 which is in good agreement with our results.

The results listed in Table 2 are probably the most accurate available for the turbulent concentration fields of axisymmetric jets, but measured values are so scattered that it is impossible to distinguish whether plotting mole fraction or mass fraction gives the best agreement for jets of different

density gases. Becker et al. [48] reviewed experimental results in the literature for concentration and passive temperature fields of air-air jets and found that even though C_1^X values seem to cluster near 0.1, the measurements show similar scatter to those given in Table 2. Despite this apparent uncertainty in C_1^X values, it was claimed [62] that a value of C_1^Y equal to 0.1 is a constant for isothermal and combusting jets. Clearly, more careful work is needed to determine whether or not a density effect is present in these studies and whether or not the use of the effective radius of Thring and Newby [58] provides a suitable correction for changes in jet centerline behavior as the density of the jet gas is changed due to molecular composition.

Table 2 also includes the constants which describe the behavior of RMS concentration fluctuations on the jet centerline (see Eqs. (5.3) and (5.4)). The agreement between the slope of the curve for our results in terms of mass fraction concentration and that found by Birch et al. [23] is excellent. These workers have concluded that RMS concentration fluctuations approach similarity faster than the average concentration. This is consistent with our finding that C_2^Y values are in better agreement than C_1^Y for the two studies. This behavior is the opposite of that found for the velocity flow field where the average flow velocity approaches similarity faster than the RMS fluctuations [63]. Both of the experiments on methane jets give C_2^Y values which are in poor agreement with the results of Becker et al. [48] for an air-air jet. It should be noted that no density correction is included in Eq. (5.4) and we are unaware of any method used to make such corrections for RMS concentration fluctuations. However, the use of the effective radius concept would improve the agreement. It is an interesting and as yet unexplained observation that the virtual origin shifts to more negative values for the RMS fluctuations as compared to average centerline concentrations.

By dividing Eq. (5.1) by Eq. (5.3) and Eq. (5.2) by Eq. (5.4) it is possible to derive equations which give the concentration fluctuation intensity (ξ) as a function of z for both mole and mass fraction measurements. For large values of z, differences in the virtual origins become insignificant and $\xi_{mole} = C_2^X/C_1^X$ and $\xi_{mass} = C_2^Y/C_1^Y$. Table 2 includes the results of these calculations for air-air and methane-air jets. Note that the fluctuation intensity is relatively independent of whether or not mole or mass fraction concentrations are used. Table 2 indicates that the asymptotic value of ξ is dependent on density and that it is larger in the case of a methane-air jet as compared to an air-air jet. Birch et al. [23] reached the same conclusion and noted that the velocity fluctuation intensity is also greater for the methane-air jet. This trend seems to hold for the limited data reported by Way and Libby [9] for an axisymmetric jet of helium into air. Even though only two downstream axial locations were investigated, these authors reported a value $\left(\tilde{Y}_{He}\right)_c/\left(\bar{Y}_{He}\right)_c$ of 0.37 at $z/r_o = 40$.

There is a paucity of measurements of skewness and kurtosis in the concentration fields of axisymmetric jets. The only results of which we are aware are due to Birch et al. [23]. These earlier results do not show the strong variations in skewness apparent in Fig. 7 for small z/r_o. Their results for $z/r_o > 20$ have values of $S \sim -0.3$ and seem relatively constant over the $z/r_o = 20$ to 60 range investigated in the current work. Our results seem to indicate an increase from $S \sim -0.6$ to $S \sim -0.35$ over the same range of z/r_o values. Despite these minor differences, the agreement of these two sets of measurements must be considered good since each study indicates a negative skewness (S = 0 for a Gaussian) of approximately the same magnitude on the jet centerline. Similar agreement is found for the kurtosis measurements

summarized in Fig. 8. Both studies find decreasing values of kurtosis which remain greater than 3 (the Gaussian value) throughout the entire range of z/r_o values investigated. The behavior of these parameters for air-air flows marked with heat are also consistent with our measurements [50,64].

At this time it is difficult to compare our power spectra, autocorrelation, and integral time scale measurements with other such measurements in the literature. As already noted, our measurements are susceptible to digital noise and fluctuations due to the short period of time for which data are collected. The general behavior that we observe for the power spectra is consistent with the results in the literature where plots of log(spectral density) versus log(frequency) give a relatively flat region at low frequencies followed by a rapid fall-off at higher frequencies. We feel that our data collection and analysis procedures can be modified in order to obtain more accurate autocorrelation measurements.

The radial profiles of average methane concentration in terms of mole and mass fractions are shown in Fig. 11. The experimental data are found to obey the Gaussian form of Eq. (5.5) quite well for values of $r/r_{1/2} < 1.5$. At larger values of $r/r_{1/2}$ the data seem to fall below the calculated curve, but definite statements are difficult due to uncertainties in the results arising from the short sampling times employed. Equations which are exactly equivalent to Eq. (5.5) have been used to model the radial concentration behavior in air-air [48], methane-air [23], and propane-air [2] jets. In addition, Shaughnessy and Morton [16] and Santoro et al. [60] have measured radial concentration profiles for air-air and 10% methane in air-air jets which are fit well by Eq. (5.5). For the case of the air-air jet studied by Becker et al. [48], the authors claimed that at large values of $r/r_{1/2}$

$\left(\bar{X}_{AIR}/\left(\bar{X}_{AIR}\right)_c < 0.08\right)$ the experimental data fit was improved by using an equation which predicts a concentration fall-off with increasing r which is faster than Gaussian. This is consistent with our observations noted above. Clearly, the shape of the radial profiles for concentration behavior are equivalent within experimental error for all axisymmetric jets investigated thus far. It should be noted that the results for a propane-air jet [2] are in terms of mole fraction concentrations and those for the methane-air jet [23] are in mass fraction terms. An analysis of the effect of transforming from mole fraction to mass fraction on the shape of the concentration radial profile indicates very little change in the overall shape of the profile, but the $r_{1/2}$ values shift to slightly smaller r values for positively buoyant jets and to larger values for negatively buoyant jets. This can be seen in Fig. 11 where $r_{1/2}$ for the mole fraction concentration is 12 mm and for the mass fraction concentration case is 11.5 mm.

Often the spreading rate of the jet is defined using $r_{1/2}$ values. For sufficient downstream distance the value of $r_{1/2}$ is found to be proportional to the distance from a virtual origin z_o . This relationship is written as

$$r_{1/2} = C_3(z - z_o) \qquad (6.1)$$

where the values of C_3 and z_o will be dependent on whether mole or mass fraction concentrations are used. Table 3 summarizes values of C_3 obtained for different jets using various experimental techniques. Dyer [2] claimed that his value of C_3 indicates the presence of a slight density effect on the spreading rate of the jet. This conclusion may be correct, but such a definite statement is difficult to justify based on the limited data of

Table 3 which indicate very little difference between the air-air and methane-air jets.

There does seem to be a density effect when concentration fluctuation RMS values along the radial direction are considered. Figure 12 shows that the normalized radial RMS values we observe are in close agreement with the methane-air results of Birch et al. [23]. One possible means of characterizing this type of measurement for different jets is to compare the values of the maximum ratio of $\tilde{X}_{max}/\tilde{X}_c$ or $\tilde{Y}_{max}/\tilde{Y}_c$ observed and the value of $r/r_{1/2}$ where it occurs. Table 4 lists the results from a number of different laboratories. Four sets of data are given for air-air jets in which passive markers were used as concentration probes. Becker et al. [48] and Shaughnessy and Morton [16] both used light scattering from particles for their measurements. There is very good agreement between these two groups for both $\tilde{X}_{max}/\tilde{X}_c$ and $r_{max}/r_{1/2}$. Antonia et al. [50] and Chevray and Tutu [51] have also studied air-air jets, but used heated air as a marker. These two groups of workers are in good agreement, but the results obtained using the two different techniques are in relatively poor agreement with the particle measurements which give lower values for $\tilde{X}_{max}/\tilde{X}_c$ and $r_{max}/r_{1/2}$. It may be that one of these techniques does not respond to turbulent fluctuations perfectly or that the markers are not totally passive. Despite this discrepancy, Table 4 shows that the ratio of $\tilde{X}_{max}/\tilde{X}_c$ and $\tilde{Y}_{max}/\tilde{Y}_c$ is greater for both methane and propane jets than for air-air jets. Due to the discrepancy in the results for the air-air jets it is impossible to state whether or not there is a density effect on the value of $r_{max}/r_{1/2}$.

Our results for the skewness and kurtosis of concentration fluctuations as a function of $r/r_{1/2}$, shown in Figs. 13 and 14, are in excellent agreement with the results of Birch et al. [23]. Both the magnitudes of the parameters and their behavior as a function of $r/r_{1/2}$ match closely. Our results are also in good agreement with those of Antonia et al. [50] for an air-air jet. The rapid increases in both skewness and kurtosis values at the edge of the jet can be understood when it is noted that the intermittency factor rapidly falls off at approximately the same values of r where the large increases occur (compare Figs. 13 and 14 with 17). In this region of the flow field, periods of time when the methane concentration is zero are averaged with those when the concentration is nonzero (this can be clearly seen in Fig. 16). Since the methane concentration cannot be negative, a sharp cut-off in the concentration distribution exists at the lower end and the skewness and kurtosis values must increase dramatically as the fraction of time during which the fluid is pure air increases.

We have been unable to find detailed integral time scale measurements as a function of r with which to compare the measurements shown in Fig. 15. However, Dyer [2] did find that T increased from 140 μs to 315 μs on going from the centerline to $r_{1/2}$ in a propane-air jet.

No measurements of intermittency in the concentration field of an axisymmetric jet have been reported, but studies using passive markers have been performed. Becker et al. [48] studied the intermittency function for an air-air jet where the intermittency decision was based on light scattering from particles. These workers found that the radial location where

$\gamma = 0.5$, $\bar{R}$, is equal to $\bar{R}/r_{1/2} = 1.78$. Using a similar technique, Shaughnessy and Morton [16] found that $\bar{R}/r_{1/2}$ was 1.52 for an air-air jet with Re = 56052 and 1.43 with Re = 31590. Chevray and Tutu [51] have performed detailed intermittency measurements in a heated air-air jet where the heat acted as a passive scalar. A value of $\bar{R}/r_{1/2} = 1.6$ can be inferred from their data. All of these values must be considered to be in good agreement with our measurement of $\bar{R}/r_{1/2} = 1.6$ since the value of $\bar{R}$ is highly dependent on the observation volume and cut-off constant used. (See discussions in Antonia et al. [50], Shaughnessy and Morton [16].)

It is difficult to compare our result for the wrinkle amplitude with the value measured by Becker et al. [48] since these workers found that the value of σ_w on the centerline is given by an equation with a different virtual origin than $r_{1/2}$. However, by assuming large values of z, a value of $\sigma_w/r_{1/2} = 0.29$ can be derived from their results. This value is in excellent agreement with the value of 0.28 determined in this study. In their study using heat as a marker, Antonia et al. [50] found that σ_w was equal to $0.3r_{1/2}$ which is also in good agreement with our results.

As noted earlier, the concentration fluctuations in the intermittent region of the flow show a distinct ramp-like structure which is clearly visible in Fig. 16. To our knowledge, this is the first observation of such structures in turbulent flows for an experiment monitoring concentration fluctuations directly. However, such structures have been found in studies using heat as a passive marker. As early as 1968 Gibson et al. [65] noted the presence of this behavior in the wake of a heated sphere where the sharp edge of the ramp occurred at the upstream end of the turbulent bulge. Similar

structures in axisymmetric jets have been found to have the leading edge of the ramp facing downstream [50]. This observation is consistent with the time record of methane concentration fluctuations shown in Fig. 16 where the sharp edges of the ramp-like structures occur at the leading or downstream edge of the turbulent bulges.

The observation of these ramp-like structures in intermittent regions of turbulent flows has resulted in a wide range of studies which are beginning to yield detailed information concerning the behavior of large scale structures. Measurements of nonzero values of skewness in the derivative of temperature with respect to z, which can be obtained from $\partial T/\partial t$ by use of Taylor's hypothesis, have been associated with these ramp-like structures. (See Gibson et al. [66] and Sreenvivasan and Tavoularis [67].) Such observations are important, since one of the predictions of Kolmogorov's concept of local isotropy [45] is that the skewness of $\partial T/\partial z$ will be zero. As might be expected, the sign of the derivative is found to depend on the type of flow configuration. The values are negative when the edge of the ramp faces downstream and positive when the face is upstream. Relations are being developed to predict the sign of the derivative based on measurements of average flow field properties [66,67].

Important clues to the nature of turbulent mixing have been derived from the work of Chevray and Tutu [51] on heated axisymmetric jets. They used highly conditioned measurements to obtain average radial velocities near the beginning and end of the turbulent bulges. These workers have found that the average direction of fluid flow is away from the center of the jet at the downstream edge of the bulges. This implies that highly concentrated gas from

the center of the jet is being "shot out" into the surrounding fluid and thus explains the sharp edge of the ramp. At the upstream end of the ramp the average flow direction of the fluid is towards the center of the jet. In this region the surrounding gas is being entrained into the jet and dilutes the jet fluid leading to the fall-off in concentration as the bulge passes the observation volume. This proposed mechanism is described in a very lucid way in the paper by Gibson et al. [66].

Figure 19 shows that, as expected, the concentration of methane in the turbulent regions is considerably higher than the unconditioned concentration when the flow is intermittent. This same general behavior has been observed in similar studies using passively marked air-air jets. Becker et al. [48] have given a numerical specification for $\left(\bar{X}_{AIR}\right)_T/\left(\bar{X}_{AIR}\right)_c$. For given $r/r_{1/2}$ values their turbulent concentrations are found to be significantly lower than those indicated in Fig. 19. For instance, at $r/r_{1/2} = 2$, this earlier work yielded a value of 0.15 for $\left(\bar{X}_{AIR}\right)_T/\left(\bar{X}_{AIR}\right)_c$, compared with a value of 0.29 taken from Fig. 19. This discrepancy is easily understood by noting that this earlier work found that the average location of the boundary of the jet occurs at $\bar{R}/r_{1/2} = 1.78$ as opposed to the value of 1.6 we have measured. Since the normalized wrinkle amplitude is nearly equal for the two jets, the value of γ at any normalized radius will be larger for the air-air jet. The radial profiles of concentration are nearly identical, which implies that at any given radial location the "turbulent fluid" must contain a higher proportion of low concentration jet fluid and the average concentration in the turbulent region will be lower. This conclusion is supported by the results of Chevray and Tutu [51] for a temperature marked jet. These workers found a normalized value of $\bar{R}/r_{1/2}$ which is nearly identical to that reported for the methane-air

jet used here. The values of $\left(\bar{X}_{AIR}\right)_T/\left(\bar{X}_{AIR}\right)_c$ (where it must be remembered it is assumed that $\bar{X}_{AIR}$ is proportional to a temperature difference) as a function of normalized radius are in very good agreement with the current measurements. For instance, at $r/r_{1/2} = 2$ these workers found a value of $\left(\bar{X}_{AIR}\right)_T/\left(\bar{X}_{AIR}\right)_c = 0.30$, which is very close to the value of 0.29 cited above. Based on these results, the current measurements of conditional concentrations must be considered in good agreement with the limited data available in the literature for passively marked air-air jets.

Data available for comparison with the conditional RMS values shown in Fig. 19 are limited to the studies of Becker et al. [48] and Antonia et al. [50]. The general behavior of the particle marked air-air jet is similar to that shown in Fig. 19. Initially, as the mixing becomes intermittent the values of $\left(\tilde{X}_{AIR}\right)_T/\left(\tilde{X}_{AIR}\right)_c$ fall below the value of $\tilde{X}_{AIR}/\left(\tilde{X}_{AIR}\right)_c$. As the value of r is increased the value of the conditioned RMS again approaches that of the unconditioned RMS and then becomes larger. The same general behavior is found for the temperature marked jet. Interestingly, Antonia et al. [50] find that the value of $\left(\tilde{X}_{AIR}\right)_T/\left(\tilde{X}_{AIR}\right)_c$ remains very nearly constant across the entire jet profile in marked contrast to the results of Fig. 19 or the particle marked air-air jet where the intensity first rises and then falls for both the conditional and conventional measurements. At this time we can offer no explanation for this difference, but will note that Antonia et al. [50] performed their study in a co-flowing stream of air where the velocity ratio of the jet to surrounding gas was considerably lower than those used in this study or the free jet used by Becker et al. [48].

The only conditionally averaged skewness and kurtosis results of which we are aware for the radial distribution of concentration fluctuations is the work of Antonia et al. [50]. These workers find nearly identical behavior for these two parameters as shown in Figs. 13 and 14. At r values where both the skewness and kurtosis are rapidly increasing due to intermittency, conditional measurements remain nearly constant. For both sets of measurements the conditioned value of skewness is positive and equal to approximately one while the kurtosis value remains slightly higher than the Gaussian value of three.

6.2 Validity of Comparisons with Other Studies

Up to this point, differences between our experimental flow conditions and those of studies with which our results are compared have not been considered in detail. Table 5 summarizes the conditions used in each of these studies for some of the parameters which might influence the measurements compared in Section 6.1. The values in the table are given in terms of the density ratio of the jet fluid to the surrounding air, the ratio of the air velocity (u_{AIR} = 0 is a free jet) to the jet velocity, and the Reynolds number corresponding to the velocity difference between the jet and surrounding flow.

From Table 5 it is clear that the experiments used for comparison purposes with the results of this work have been performed under widely varying conditions. Despite these differences in flow conditions, very good agreement is found between our results and these earlier studies. In particular, the agreement between our results and those of Birch et al. [23] is very good, despite the fact that their jet was a free jet with a Reynolds number four times greater than that used for this work. The large differences

in virtual origins recorded in Table 2 also indicate that the initial conditions at the jet nozzles were very different for the two jets.

It is obvious that the use of an enclosure and a coflow of surrounding gas must change the concentration field behavior of the axisymmetric jet used in this study as compared to that of a free jet. As the jet slows down due to turbulent mixing with its surroundings, it will eventually decay to a velocity where it must respond to the coflow of air. The jet is also constantly expanding and will eventually fill the entire enclosure. However, in the downstream regions of the flow where we have made measurements, the effects of the coflowing surrounding gas and the enclosure do not seem strong enough to modify the concentration field in an experimentally verifiable way. This is consistent with our observation that the velocity behavior of the jet is the same with and without the enclosure. The radial profile of the jet was studied at an axial position where the jet has a maximum radius of ~29 mm. (The outer edge of the jet spends 99.9% of the time within this distance of the centerline, see Fig. 18.) Since the shortest distance from the jet centerline to the walls of the enclosure is 50.9 mm, it is not surprising that the presence of the walls does not modify the behavior of the jet in a measurable way. The absence of an effect due to the coflowing surrounding gases on the averaged properties of a jet at comparable downstream distances to those employed here has been noted by Shaughnessy and Morton [16]. These workers found that their results for a coflowing air-air jet were in very good agreement with those of Becker et al. [48] for the corresponding free jet.

Ebrahimi and Kleine [62,68] have given a formula for the variation of C_1^Y with Re which can be written as

$$C_1^Y = (1.3(Re/10^4) + 6)^{-1} \qquad (6.2)$$

Table 2 compares values of C_1^Y from four different measurements where the Reynolds number varies from 3770 to 54,000. Using Eq. (6.2), the expected variation in C_1^Y is from 0.154 to 0.077. The results summarized in Table 2 indicate a much smaller variation than this. Based on the results of our measurements and comparisons with others in the literature, we feel that a small Reynolds number effect may be present for values of C_1^Y, but that this effect is hidden by variations in values of C_1^Y due to experimental conditions. Shaughnessy and Morton [16] found very little effect on jet properties on going from Re = 56,050 to Re = 31,590. However, they did note a small, but reproducible, decrease in the half-widths of the average velocity, average concentration, and the normalized value of $\bar{R}$ as Re was lowered. Antonia et al. [50] have reported a similar behavior, but the results may not be comparable with those of the other jets in Table 5 due to the relatively high values of u_{AIR}/u_{JET} used in this work. Effects of Re differences on the other properties of the concentration field evaluated in this study have not been reported. All of the evidence cited above indicates that while small effects of Re may be present in these measurements, these effects are not strong enough to invalidate the comparison of our results with other studies discussed in Section 6.1.

The effects of density differences on the behavior of the average concentration field and the RMS have already been discussed in Section 6.1. The concept of an effective radius used in Eq. (5.2) is expected to compensate for density differences between jet fluids for comparisons of the axial behavior of average mass fraction concentration, but the variations in the

measured results among different studies are so large that this has not been verified. A strong effect does appear in the behavior of the RMS concentration fluctuation. Careful studies should be performed to confirm and characterize this density effect. The presence or absence of effects due to density differences on the other properties of the flow field reported in this study cannot be verified due to insufficient data for comparison.

On the basis of the very good agreement of the measured properties of the concentration flow field from this study and those in other studies and the lack of experimental evidence indicating strong modifications of the field (with the possible exception of those due to the effects of jet density), we conclude that the measurements reported in Section 5.2 and Section 5.3 are reasonable and give an accurate description of the concentration field of an axisymmetric jet.

6.3 Applicability of Rayleigh Light Scattering as a Scalar Probe of Turbulent Flow Fields

In the past, many different measurement techniques have been used to make scalar measurements in turbulent flow fields. Some of these techniques have been discussed briefly in Section 1.2. All of these techniques have serious disadvantages and no one experimental method has dominated the field. Concentration and temperature measurement methods have lagged far behind the corresponding velocity measurements where hot-wire and laser anemometry have provided easily implemented and accurate velocity determinations.

This study has been designed to demonstrate the feasibility of using laser Rayleigh light scattering as a concentration probe in simple turbulent flow systems. The Rayleigh technique has previously been shown to be a powerful means of monitoring mass density, number density, and temperature fields in carefully selected complex turbulent reaction systems (see discussion in Section 2.2). As suggested by the pioneering studies of Graham et al. [1] and Dyer [2], the work reported here has proven that Rayleigh light scattering is an excellent technique for performing quantitative time- (~200 μs) and spatially-resolved (~0.0003 mm^3) measurements in a two gas turbulent flow system. A wide variety of turbulence properties have been investigated and the results have been shown to be in excellent agreement with those in the literature which were measured using independent techniques.

A necessary requirement for this technique to have a wide applicability is that it be useful for a large number of different gas mixtures. One of the reasons methane was chosen for this study is that it does not have an unusually strong Rayleigh scattering cross section relative to that of air. Most gas pairs have scattering cross section ratios at least as large as that for methane-air, $\sigma_{CH_4}/\sigma_{AIR} = 2.34$, and many are considerably higher. For instance, the propane-air combination has a ratio of 13.5. Furthermore, most gases have scattering cross sections which are the same order of magnitude (the very small cross section for helium is an exception) as those for air and methane. This implies that the present experimental arrangement can be used to study a wide variety of two component turbulent flows with temporal and spatial resolution comparable to those found for this study. Of course, some combinations of gases will not be suitable due to their having cross sections which are nearly identical. In order to determine whether or not a particular

binary gas combination is suitable for study, an analysis similar to that developed in Section 2.3 can be performed. Our results indicate that this analysis will only provide an order of magnitude estimate of signal and noise levels, but it should be possible to relate the results of the calculation to those combinations of gases for which experiments have been previously done in order to obtain a more accurate estimate of expected signal and noise levels.

Even though the experimental apparatus developed for this study provides concentration measurements with high spatial and temporal resolution, it is easy to imagine experiments for which improved signal to noise ratios or higher temporal and/or spatial resolution would be required. Earlier analysis in Section 2.3 has shown that by far the most important factor which limits the Rayleigh light scattering technique is the relative weakness of the scattering and the resulting noise in the detected signal due to Poisson statistics. In order to obtain the optimum quality of information from such a measurement, the researcher is forced to make compromises concerning spatial and temporal resolution since the signal to noise ratio decreases as the observation volume and averaging time decrease. As an example, it would be possible to increase the cut-off frequency used in this work by a factor of 4, while maintaining a constant signal to noise ratio, by opening the slits to 1 mm. In many cases, observation of turbulent fluctuations within a cylinder of 1 mm length would provide sufficient spatial resolution and the faster response time would allow higher velocity flows to be investigated.

A second means of improving signal to noise ratios in this type of study is to increase the intensity of light reaching the detector by improving the experimental system. This can be accomplished by increasing the laser power

within the observation volume and/or improving the transmission and efficiency of the collection and filtering optics. Even though more powerful CW lasers are available commercially, the high cost and complexity of such lasers compared to the system used here does not make this approach to increasing laser power attractive. However, it is possible to increase the laser power in the scattering volume by using a multipass mirror system or placing the observation volume within the laser cavity where laser power levels are considerably higher. Either of these improvements can be expected to increase laser intensity levels within the observation volume by factors of 10-100. By more careful design of the optical system and use of AR coated optical components throughout, another increase of 2-3 in light reaching the detector can be expected. The gains in signal to noise ratio are attained by the use of more complex and costly optical components.

At this point it is proper to consider what types of additional quantitative scalar measurements can be made in turbulent flows using the Rayleigh light scattering technique as developed here. It is possible to use the same apparatus to investigate turbulent mixing of heated or cooled jets of a single gas issuing into the same gas. The variable which is fluctuating in this case is temperature. Since changes in temperature result in density variations (for constant pressure), Eq. (2.10) shows that for a single component flow the Rayleigh scattering intensity will be inversely proportional to the absolute temperature. For the case of a heated air-air flow, the jet would need to be at ~650 K in order to observe signal to noise levels comparable to those of the methane-air jet. Similarly, a jet cooled to 150 K would provide similar signal levels. Studies such as those outlined here would provide information concerning turbulent mixing of gases when temperature differences cannot be considered to be passive.

The discussion of Section 2.1 has shown that an analysis of the scattered Rayleigh light in terms of its polarization components, $I_{\parallel}$ and $I_{\perp}$, yields an additional independent variable which is characteristic of the molecular composition. Subject to the constraints on Rayleigh scattering cross sections and depolarization ratios previously discussed, the measurement of these two intensities allows the mole fractions of a three component isothermal gas or the temperature and concentration of a two component nonisothermal system to be uniquely determined. Since a typical value of $\rho = I_{\perp}/I_{\parallel}$ is 0.01, the intensity of the perpendicular component is expected to be ~100 times smaller than the total scattering intensity. This implies that for the conditions used in this study that either the time or spatial resolution would have to be severely sacrificed in order to employ polarized Rayleigh light scattering as a probe for quantitative measurement of three scalar quantities. However, methods of significantly increasing the intensity of detected scattered light have been described above. The use of these techniques would allow intensity measurements of the polarized components to provide simultaneous values of three scalar quantities with temporal and spatial resolution similar to those reported in the current study.

We conclude from the results of this study and the discussions above that Rayleigh scattering offers a useful and accurate method for quantitative scalar measurements in many simple flow systems. When its applications to global measurements discussed in Section 2.2 are included, it is clear that Rayleigh scattering can become a powerful tool for the analysis of scalar properties in turbulent flow fields.

6.4 Rayleigh versus Raman Scattering as a Scalar Probe

Due to the nature of the techniques, turbulence experimenters will often be required to choose between Rayleigh and Raman light scattering as nonobtrusive probes for turbulent flow systems. The choice of type of scattering measurements must be based on the nature of the flow and the properties which are to be determined. Peterson [13] has indicated in his review that Raman scattering is widely accepted as a flow diagnostic while experiments using Rayleigh scattering are not widely used. We feel that this is unfortunate since there are many experimental conditions for which Rayleigh scattering should be superior due to its large cross section relative to those for Raman scattering. For flow systems where either Rayleigh or Raman scattering can be used, such as the flow studied here, two component heated flows, three component isothermal flows and the reacting flows described in Section 2.2, Rayleigh scattering should offer substantial advantages over Raman scattering. Consider the application discussed in this work. Birch et al. [23] have performed essentially the same study using Raman techniques. These workers reported point measurements for the average, unmixedness, skewness, kurtosis, concentration probability functions, and autocorrelation functions of the methane concentration fluctuations in the jet. Our analysis indicates that, with the exception of the autocorrelation functions, the measurements described in Section 5.2 are in excellent agreement and of comparable quality with those of this earlier work. These workers have not reported the time required for making a single point measurement in the flow, but since Raman scattering is expected to be at least 1000 times weaker than Rayleigh scattering, the time required to obtain a measurement with equivalent signal to noise should be at least 1000 times longer. This implies a time

approaching an hour to make a single measurement which was performed in three seconds using Rayleigh scattering. These considerations are not only important from an efficiency viewpoint. In cases where the flow of expensive gases are being studied it is important to limit experimental time for cost effectiveness. The above discussion is with regard to CW Raman experiments. Similar constraints will apply to experiments using pulsed lasers.

When it is noted that Rayleigh scattering also allows time-resolved studies and that the experimental requirements for Rayleigh scattering are less stringent (i.e., no spectrometer is required for Rayleigh scattering), it is clear that Rayleigh scattering is the superior technique for applications where its use is suitable. Examples where Rayleigh scattering cannot be used are systems where a large number of different gases must be monitored or where intense scattering from particles (such as soot) or the apparatus does not allow the elastic scattering to be observed. In these cases, Raman scattering provides an excellent alternative.

6.5 Final Remarks

This work has presented a detailed description and investigation of laser induced Rayleigh scattering as a concentration probe in binary mixtures of isothermal turbulent flows. It has been demonstrated that the technique can be used to provide detailed properties concerning the concentration flow field. In addition, detailed information concerning the concentration field of an axisymmetric jet has been provided which should aid in a more complete understanding of turbulent mixing. In the near future we hope to perform detailed density effect studies on this flow configuration using Rayleigh scattering as the probe.

Even though we feel that Rayleigh scattering has been demonstrated to be a powerful technique, there are several improvements which would make it more universally useful for turbulence studies. Among these is the use of polarization effects to allow an additional scalar property to be measured. It should also be possible to extend the technique to two dimensions as has been done for particle nephelometry [18] and Raman scattering [21].

A major conclusion of this paper must be that none of the current techniques for providing scalar measurements in turbulent flows approximate those of the ideal probe described at the beginning of Section 1.2. However, it is also clear that by judicious choice, an experimenter can find techniques for performing these measurements with an accuracy and detail which has only been possible recently. In this context, the Rayleigh light scattering technique evaluated in this paper is an important addition to the turbulence researcher's arsenal of probes for scalar measurements.

7. ACKNOWLEDGMENTS

We wish to acknowledge Dr. Bernard McCaffrey of the Center for Fire Research for performing the velocity measurements reported in this work. We have also been aided by helpful discussions with Dr. Howard Baum of the Center for Fire Research and Drs. James McMichael and Patrick Purtell from the Center for Chemical Engineering.

8. REFERENCES

[1] Graham, S. C.; Grant, A. J.; Jones, J. M. Transient molecular concentration measurements in turbulent flows using Rayleigh light scattering. AIAA J. 12(8): 1140-1142; 1974 August.

[2] Dyer, T. M. Rayleigh scattering measurements of time-resolved concentration in a turbulent propane jet. AIAA J. 17(8): 912-914; 1979 August.

[3] Hinze, J. O.; van der Hegge Zijnen, B. G. Transfer of heat and matter in the turbulent mixing zone of an axially symmetrical jet. App. Sci. Res. A1: 435-461, 1947.

[4] Forstall, Jr., W.; Shapiro, A. H. Momentum and mass transfer in coaxial gas jets. J. Appl. Mech. 17: 399-408; 1950 December.

[5] Corrsin, S.; Uberoi, M. S. Further experiments on the flow and heat transfer in a heated turbulent air jet. NACA TN 1865; 1949 April. 61 p.

[6] Corrsin, S.; Uberoi, M. S. Further experiments on the flow and heat transfer in a heated turbulent air jet. NACA Rep. 998; 1950. 17 p.

[7] Chevray, R.; Tutu, N. K. Simultaneous measurements of temperature and velocity in heated flows. Rev. Sci. Ins. 43(10): 1417-1421; 1972 October.

[8] Way, J.; Libby P. A. Hot-wire probes for measuring velocity and concentration in helium-air mixtures. AIAA J. 8(5): 976-978; 1970 May.

[9] Way, J.; Libby, P. A. Application of hot-wire anemometry and digital techniques to measurements in a turbulent helium jet. AIAA J. 9(8): 1567-1573; 1971 August.

[10] McQuaid, J.; Wright, W. The response of a hot-wire anemometer in flows of gas mixtures. Int. J. Heat Mass Trans. 16(4): 819-828; 1973 April.

[11] McQuaid, J.; Wright, W. Turbulence measurements with hot-wire anemometry in non-homogeneous jets. Int. J. Heat Mass Trans. 17(2): 341-349; 1974 February.

[12] Brown, G. L.; Rebollo, M. R. A small, fast-response probe to measure composition of a binary gas mixture. AIAA J. 10(5): 649-652; 1972 May.

[13] Peterson, C. W. A survey of the utilitarian aspects of advanced flowfield diagnostic techniques. AIAA J. 17(12): 1352-1360; 1979 December.

[14] Rosensweig, R. E.; Hottel, H. C.; Williams, G. C. Smoke-scattered light measurements of turbulent concentration fluctuations. Chem. Eng. Science 15(1,2): 111-129; 1961 July.

[15] Becker, H. A.; Hottel, H. C.; Williams, G. C. On the light scatter technique for the study of turbulence and mixing. J. Fluid Mech. 30(2): 259-284; 1967 November 9.

[16] Shaughnessy, E. J.; Morton, J. B. Laser light-scattering measurements of particle concentration in a turbulent jet. J. Fluid Mech. 80(1): 129-148; 1977 April 4.

[17] Becker, H. A. Mixing, concentration fluctuations, and marker nephelometry, in Studies in Convection, Vol. 2. B. E. Launder, ed. New York, NY: Academic Press; 1977. 45-139.

[18] Long, M. B.; Chu, B. T.; Chang, R. K. Instantaneous two-dimensional gas concentration measurements by light scattering. AIAA J. 19(9): 1151-1157; 1981 September.

[19] Lederman, S.; Bornstein, J. Application of Raman effect to flowfield diagnostics, in Progress in Astronautics and Aeronautics, Vol. 34, Instrumentation for Airbreathing Propulsion. A. E. Fuhs and M. Kingery, eds. Cambridge, MA: The MIT Press; 1974. 283-296.

[20] Drake, M. C.; Lapp, M.; Penny, C. M.; Warshaw, S.; Gerhold, B. W. Measurements of temperature and concentration fluctuations in turbulent diffusion flames using pulsed Raman spectroscopy. Eighteenth Symposium (International) on Combustion. Pittsburgh, PA: The Combustion Institute; 1981. 1521-1531.

[21] Webber, B. F.; Long, M. B.; Chang, R. K. Two-dimensional average concentration measurements in a jet flow by Raman scattering. Appl. Phys. Lett. 35(2): 119-121; 1979 July 15.

[22] Birch, A. D.; Brown, D. R.; Dodson, M. G.; Thomas, J. R. The determination of gaseous turbulent concentration fluctuations using Raman photon correlation spectroscopy. J. Phys. D: Appl. Phys. 8(14): L167-L170; 1975 October 1.

[23] Birch, A. D.; Brown, D. R.; Dodson, M. G.; Thomas, J. R. The turbulent concentration field of a methane jet. J. Fluid Mech. 88(3): 431-449; 1978 October 13.

[24] Smith, J. A.; Driscoll, J. F. The electron-beam fluorescence technique for measurements in hypersonic turbulent flows. J. Fluid Mech. 72(4): 695-719; 1975 December 23.

[25] McCartney, E. J. Optics of the atmosphere. New York: John Wiley & Sons; 1976. 408 p.

[26] Robben, F. Comparison of density and temperature measurement using Raman scattering and Rayleigh scattering in Combustion measurements in jet propulsion systems. R. Goulard, ed., Proceedings of a Project SQUID workshop; Purdue University. 179-195. 1975 May 22-23.

[27] Pitz, R. W.; Cattolica, R.; Robben, F.; Talbot, L. Temperature and density in a hydrogen-air flame from Rayleigh scattering. Com. Flame 27(3): 313-320; 1976 December.

[28] Schefer, R. W.; Robben, F.; Cheng, R. K. Catalyzed combustion of H_2/air mixtures in a flat-plate boundary layer: I. Experimental results. Com. Flame 38(1): 51-63; 1980 May.

[29] Cheng, R. K.; Bill, Jr., R. G.; Robben, F. Experimental study of combustion in a turbulent boundary layer. Eighteenth Symposium (International) on Combustion. Pittsburgh, PA: The Combustion Institute; 1981. 1021-1029.

[30] Bill, Jr., R. G.; Namer, I.; Talbot, L.; Cheng, R. K.; Robben, F. Flame propagation in grid-induced turbulence. Com. Flame 43(3): 229-242; 1981 December.

[31] Dandekar, K. V. Velocity and density measurements in premixed turbulent flames. Ph.D. dissertation, Cornell University; 1981. 223 p.

[32] Gouldin, F. C.; Dandekar, K. V. Time resolved density measurements in premixed turbulent flames. AIAA paper no. 82-0036; 1982.

[33] Müller-Dethlefs, K.; Weinberg, F. J. Burning velocity measurements based on laser Rayleigh scattering. Seventeenth Symposium (International) on Combustion. Pittsburgh, PA: The Combustion Institute; 1979. 985-992.

[34] Rambach, G. D.; Dibble, R. W.; Hollenbach, R. E. Velocity and temperature measurements in turbulent diffusion flames. SAND 79-8775, Sandia Laboratories, Livermore, CA; 1979.

[35] Dibble, R. W.; Hollenbach, R. E.; Rambach, G. D. Temperature measurement in turbulent flames via Rayleigh scattering. Laser Probes for Combustion Chemistry. D. R. Crosley, ed. Washington, D.C.: American Chemical Society; 1980. 435-441.

[36] Dibble, R. W.; Hollenbach, R. E. Laser Rayleigh thermometry in turbulent flames. SAND 80-8623, Sandia Laboratories, Livermore, CA; 1980.

[37] Dibble, R. W.; Hollenbach, R. E. Laser Rayleigh thermometry in turbulent flames. Eighteenth Symposium (International) on Combustion. Pittsburgh, PA: The Combustion Institute; 1981. 1489-1499.

[38] Dibble, R. W.; Rambach, G. D.; Hollenbach, R. E.; Ringland, J. T. Simultaneous measurement of velocity and temperature in flames using LDV and CW laser Rayleigh thermometry. SAND 81-8800, Sandia Laboratories, Livermore, CA; 1981.

[39] Schefer, R. W.; Dibble, R. W.; Driscoll, J. F. Mass fluxes $\overline{\rho'\mu'}$ and $\overline{\rho'\omega'}$ measured in a turbulent nonpremixed flame. Presented at 1982 Spring Meeting of the Western States Section of the Combustion Institute, paper WSS/CI 82-35. University of Utah, Salt Lake City, Utah; 1982 April 5-6.

[40] Robben, F. Noise in the measurement of light with photomultipliers. App. Optics 10(4): 776-796; 1971 April.

[41] Brown, G. L.; Roshko, A. On density effects and large structures in turbulent mixing layers. J. Fluid Mech. 64(4): 775-816; 1974 July 24.

[42] Pike, E. R. Photon statistics. Riv. Nuovo Cimento 1 (Numero Speciale): 277-314; 1969.

[43] Brigham, E.O., The fast Fourier transform. Englewood Cliffs, NJ: Prentice-Hall, Inc.; 1974. 252 p.

[44] Cooley, J. W.; Tukey, J. W. An algorithm for the machine calculation of complex Fourier series. Math. Comput. 19(90): 297-301; 1965 April.

[45] Bradshaw, P., An introduction to turbulence and its measurement. New York: Pergamon Press; 1971. 218 p.

[46] Schon, J. P.; Charnay, G. Conditional sampling in Measurement of unsteady fluid dynamic phenomena, B. E. Richards, ed. Washington, D.C.: Hemisphere Publishing Company; 1977. 291-325.

[47] Becker, H. A.; Hottel, H. C.; Williams, G. C. Concentration intermittency in jets in Tenth Symposium (International) on Combustion. Pittsburgh, PA: The Combustion Institute; 1965. 1253-1263.

[48] Becker, H. A.; Hottel, H. C.; Williams, G. C. The nozzle-fluid concentration field of the round, turbulent, free jet. J. Fluid Mech. 30(2): 285-303; 1967 November 9.

[49] Konrad, J. H. An experimental investigation of mixing in two-dimensional turbulent shear flows with applications to diffusion-limited chemical reactions. Project SQUID tech. report CIT-8-PU; 1976 December. 110 p.

[50] Antonia, R. A.; Prabhu, A.; Stephenson, S. E. Conditionally sampled measurements in a heated turbulent jet. J. Fluid Mech. 72(3): 455-480; 1975 December 9.

[51] Chevray, R.; Tutu, N. K. Intermittency and preferential transport of heat in a round jet. J. Fluid Mech. 88(1): 133-160; 1978 September 13.

[52] Hedley, T. B.; Keffer, J. F. Turbulent/non-turbulent decisions in an intermittent flow. J. Fluid Mech. 64(4): 625-644; 1974 July 24.

[53] Antonia, R. A.; Atkinson, J. D. Use of a pseudo-turbulent signal to calibrate an intermittency measuring circuit. J. Fluid Mech. 64(4): 679-699; 1974 July 24.

[54] Goldschmidt, V. W.; Mulej, D.; Ajagu, C. O. The velocity of the turbulent/non-turbulent interface in a plane jet in Symposium on turbulence, 5th, G. K. Patterson; J. L. Zakin, ed.; 1977 October 3-5; University of Missouri-Rolla; Princeton, NJ: Science Press; 1979. 427-434.

[55] Becker, H. A.; Hottel, H. C.; Williams, G. C. Mixing and flow in ducted turbulent jets in Ninth Symposium (International) on Combustion. Pittsburgh, PA: The Combustion Institute; 1963. 7-20.

[56] Hecht, E.; Zajac, A. Optics. Reading, MA: Addison-Wesley Publishing Company; 1974. 565 p.

[57] Landolt-Börnstein. Zahenwerte und Funktionen aus Physik, Chemie, Astronomie, Geophysik, und Technik, II Band, 8 Teil, Optische Konstanten. Berlin: Springer-Verlag; 1962.

[58] Thring, M. W.; Newby, M. P. Combustion length of enclosed turbulent jet flames. Fourth Symposium (International) on Combustion. Pittsburgh, PA: The Standing Committee on Combustion; 1953. 789-796.

[59] Wilson, R. A. M.; Danckwerts, P. V. Studies in turbulent mixing - II. A hot jet. Chem. Eng. Science 19: 885-895; 1964.

[60] Santoro, R. J.; Semerjian, H. G.; Emmerman, P. J.; Goulard, R. Optical tomography for flow field diagnostics. Int. J. Heat Mass Trans. 24(7): 1139-1150; 1981 July.

[61] Bradshaw, P. The effect of initial conditions on the development of a free shear layer. J. Fluid Mech. 26(2): 225-236; 1966 October.

[62] Ebrahimi, I.; Kleine, R. The nozzle fluid concentration fluctuation field in round turbulent free jets and jet diffusion flames. Sixteenth Symposium (International) on Combustion. Pittsburgh, PA: The Combustion Institute; 1977. 1711-1723.

[63] Wygnanski, I.; Fiedler, H. Some measurements in the self-preserving jet. J. Fluid Mech. 38(3): 577-612; 1969 September 18.

[64] Venkataramani, K. S.; Tutu, N. K.; Chevray, R. Probability distributions in a round heated jet. Phys. Fluids 18(11): 1413-1420; 1975 November.

[65] Gibson, C. H.; Chen, C. C.; Lin, S. C. Measurements of turbulent velocity and temperature fluctuations in the wake of a sphere. AIAA J. 6(4): 642-649; 1968 April.

[66] Gibson, C. H.; Friehe, C. A.; McConnell, S. O. Structure of sheared turbulent fields. Phys. Fluids 20(10): S156-S167; 1977 October.

[67] Sreenivasan, K. R.; Tavoularis, S. On the skewness of the temperature derivative in turbulent flows. J. Fluid Mech. 101(4): 783-795; 1980 December 29.

[68] Ebrahimi, I.; Kleine, R. Konzentrationsfelder in isothermen Luft-Freistrahlen. Forsch. Ing. - Wes. 43(1): 25-30; 1977.

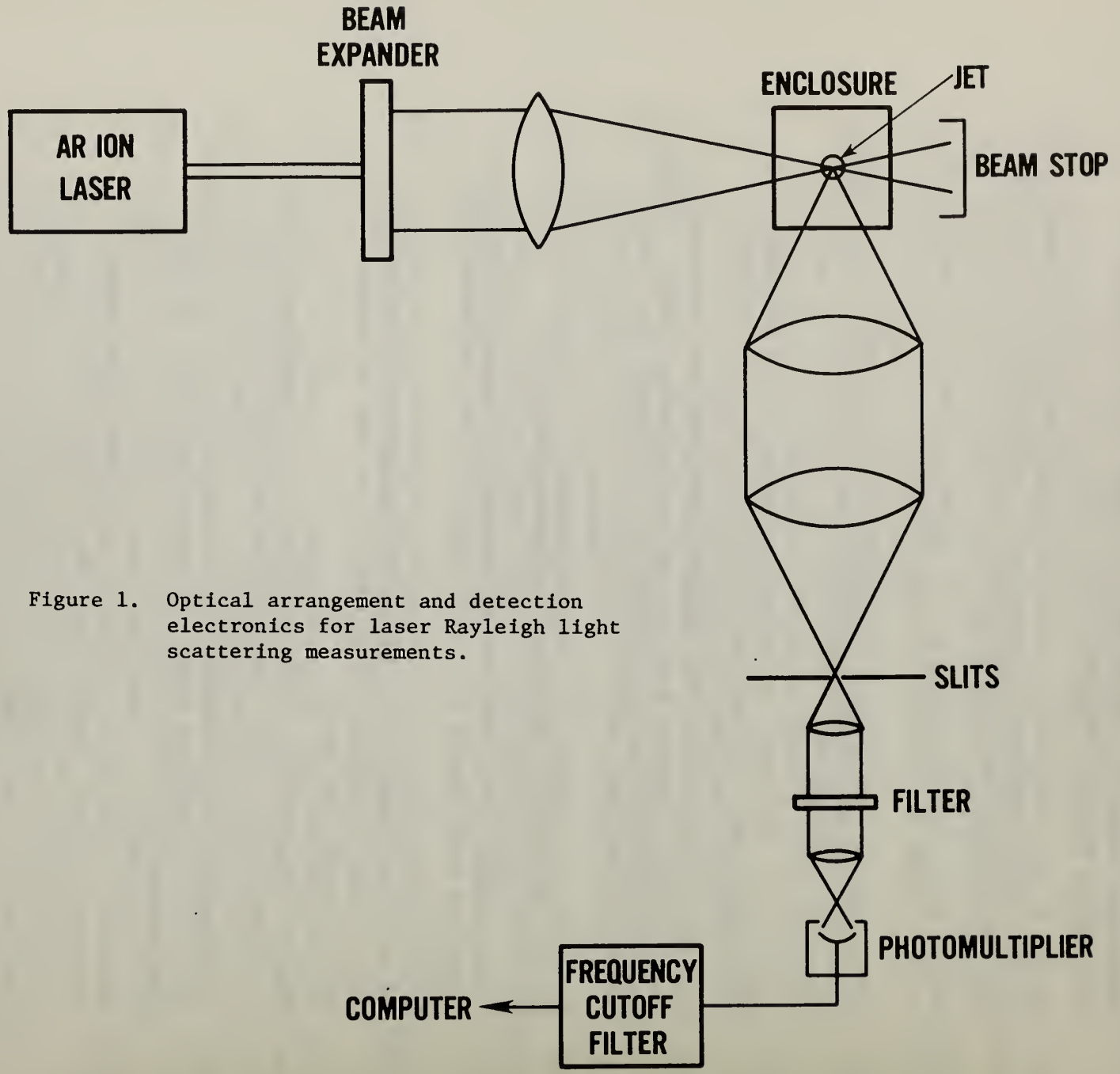

Figure 1. Optical arrangement and detection electronics for laser Rayleigh light scattering measurements.

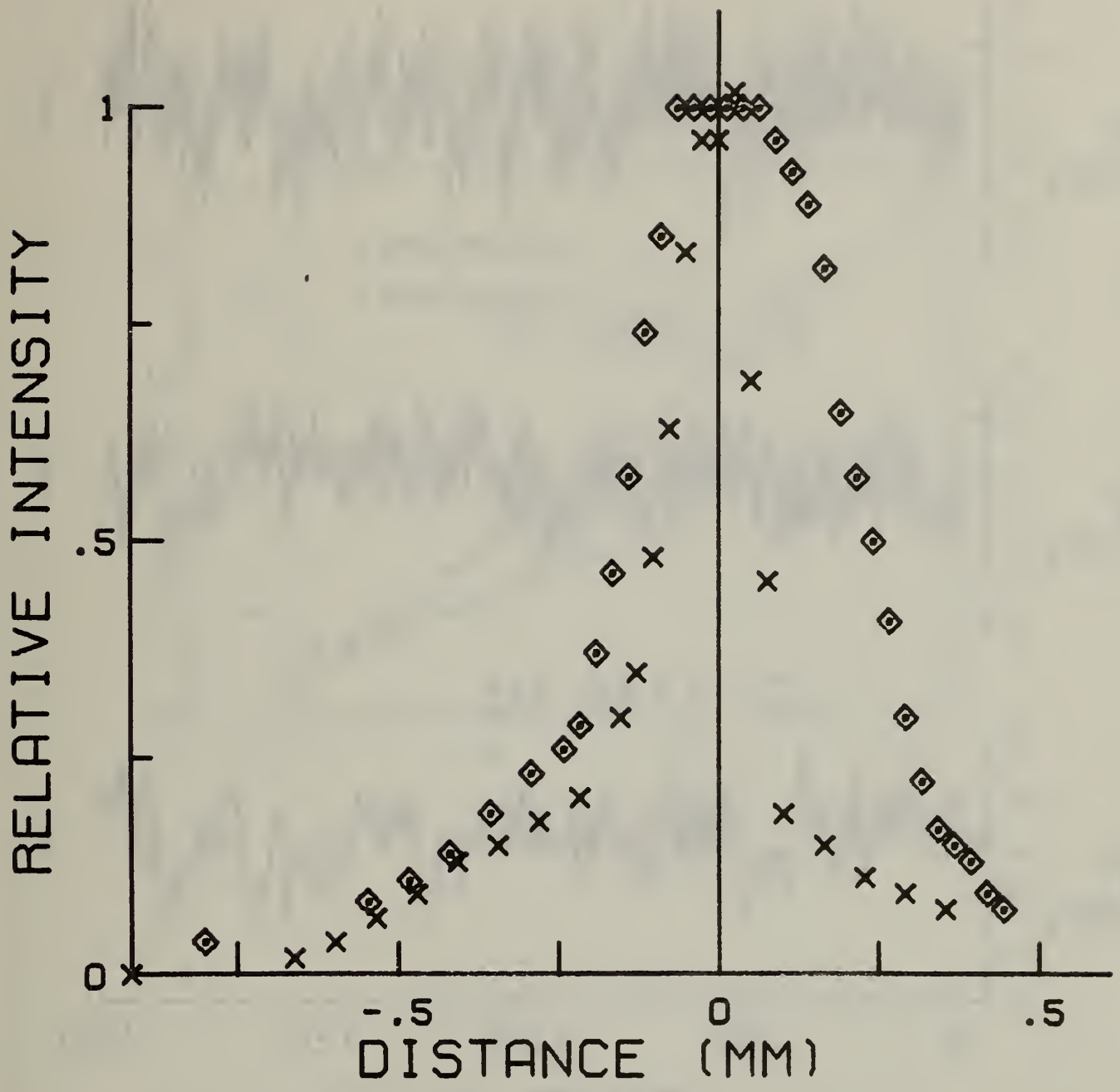

Figure 2. Detected light intensity as a function of position for a back-illuminated pinhole translated along the laser beam propagation direction. The symbols represent data for 0.2 mm (X) and 0.4 mm (◇) slit widths.

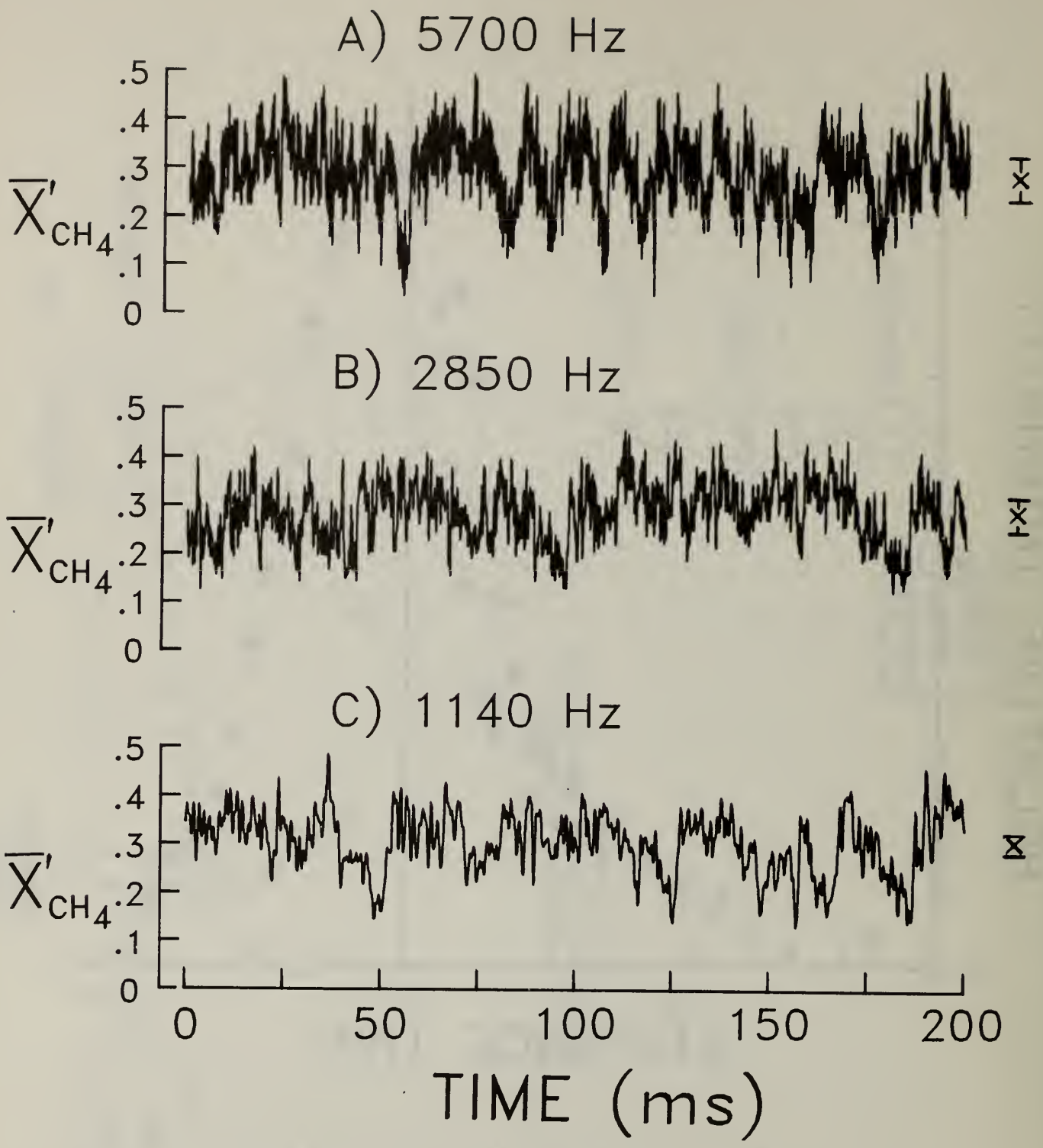

Figure 3. Appearance of data records for time-resolved light scattering measurements as a function of cut-off frequency. The measurement volume is located on the jet axis at $z/r_o = 35$. The vertical axis indicates methane concentrations which are uncorrected for photon statistics. Average methane concentrations for the entire data sets are indicated by X and the expected RMS fluctuations ($\pm$ 1 σ) due only to photon statistics are indicated by the bars.

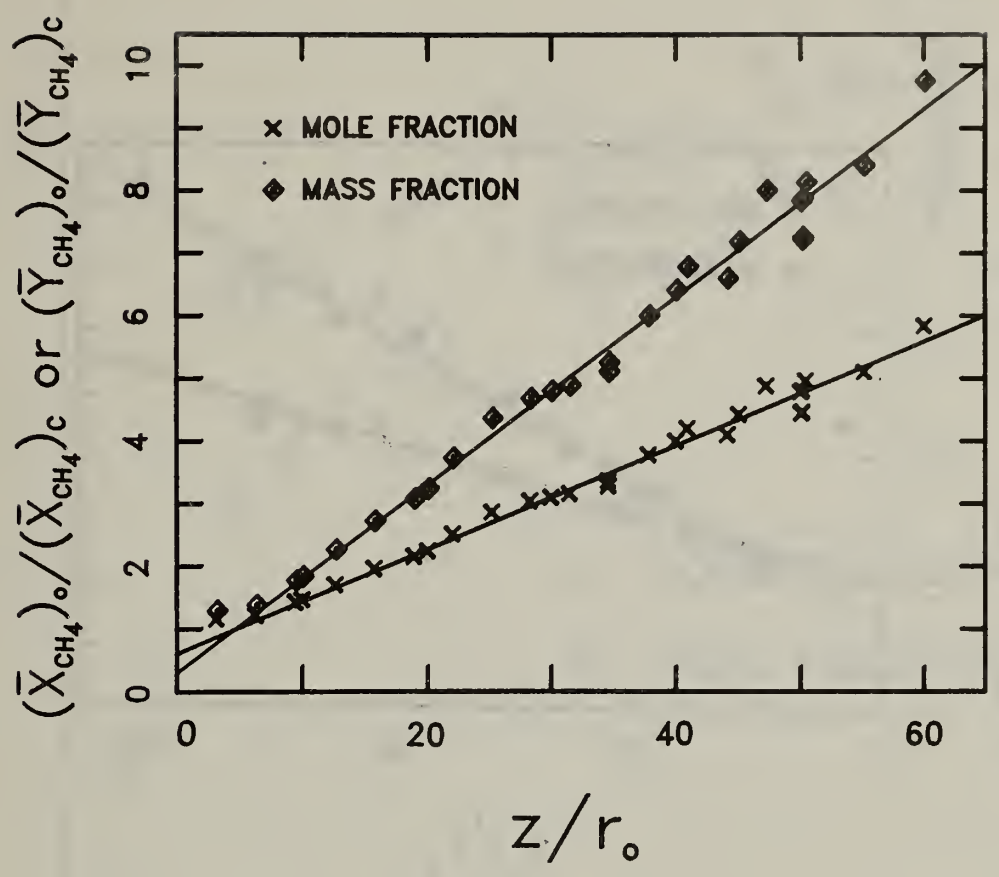

Figure 4. Values of $\left(\overline{X}_{CH_4}\right)_o / \left(\overline{X}_{CH_4}\right)_c$ and $\left(\overline{Y}_{CH_4}\right)_o / \left(\overline{Y}_{CH_4}\right)_c$ are plotted as a function of z/r_o. Solid lines are the results of linear least squares fits for measurements taken at $z/r_o \geq 20$.

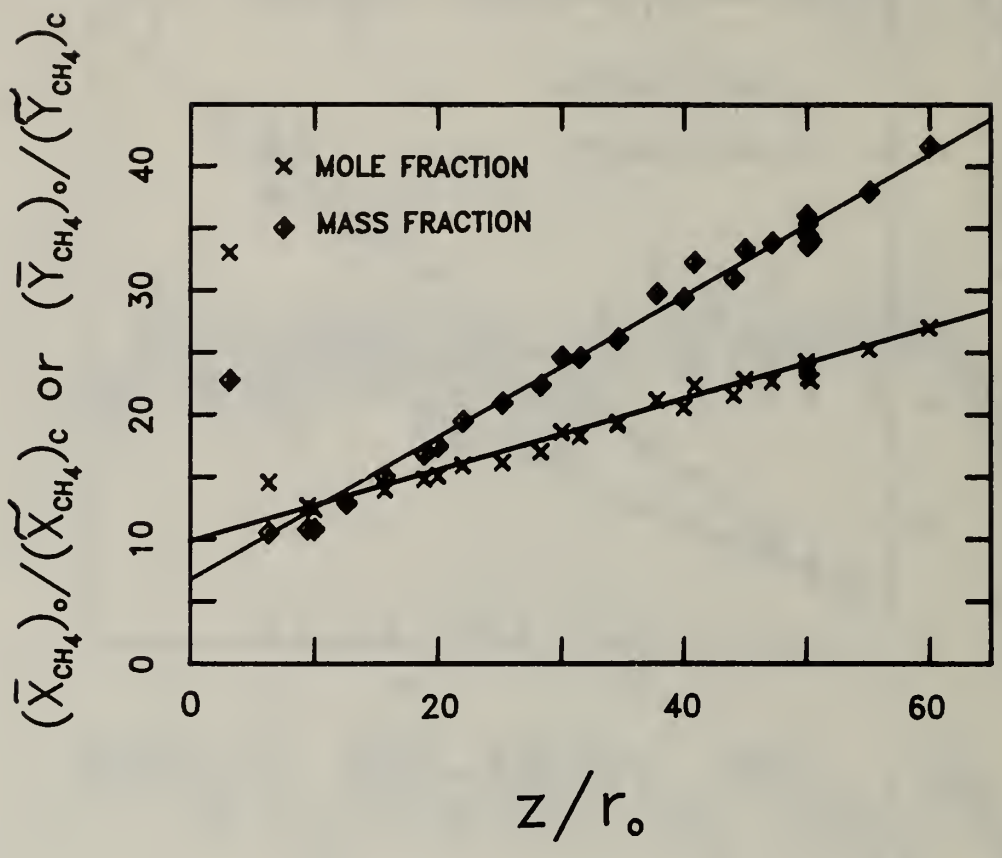

Figure 5. Values of $\left(\bar{X}_{CH_4}\right)_o/\left(\tilde{X}_{CH_4}\right)_c$ and $\left(\bar{Y}_{CH_4}\right)_o/\left(\tilde{Y}_{CH_4}\right)_c$ are plotted as a function of z/r_o. Solid lines are the results of linear least squares fits for measurements taken at $z/r_o \geq 20$.

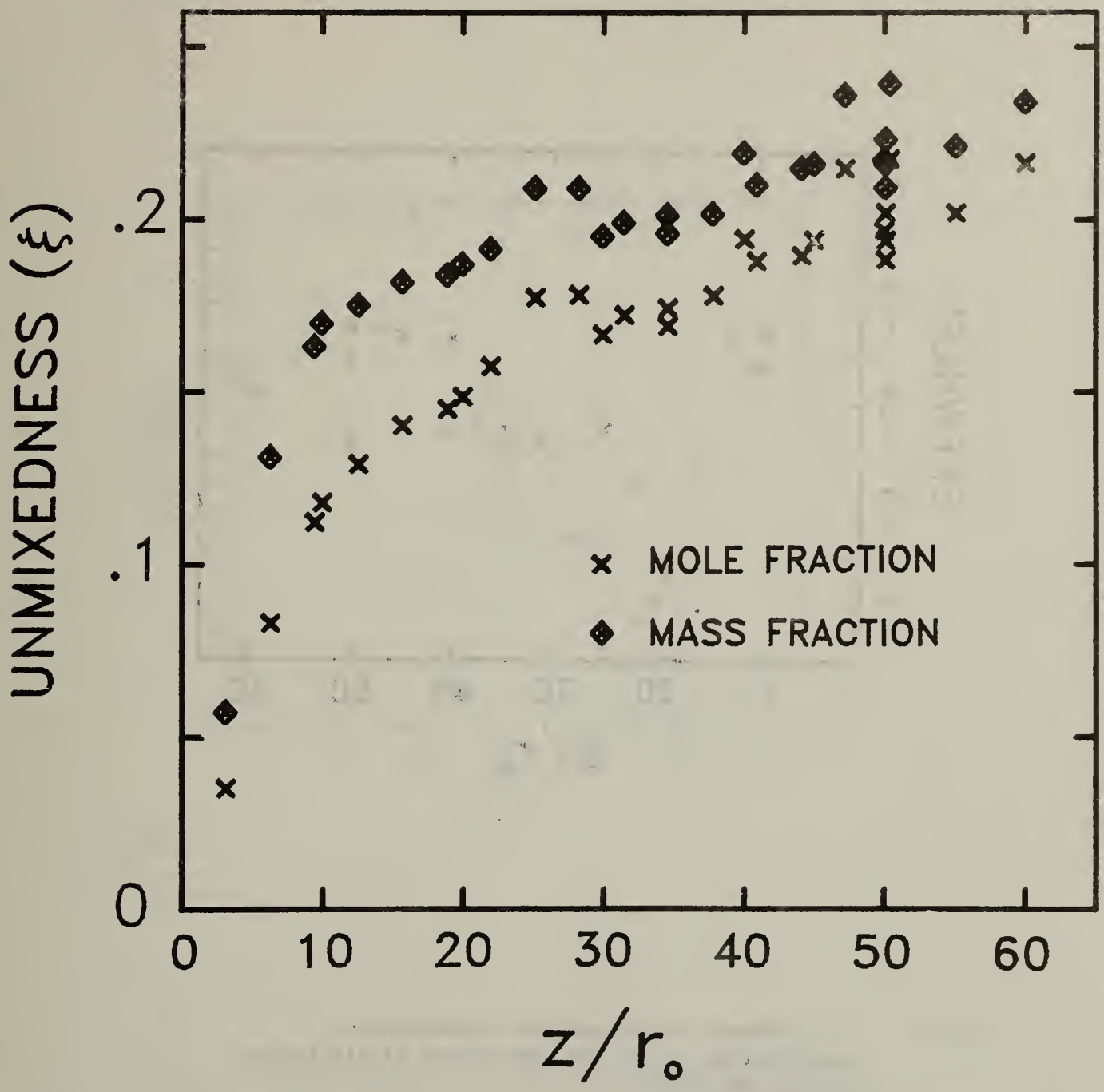

Figure 6. Unmixedness of methane concentration on the jet centerline in mole and mass fraction terms is plotted as a function of z/r_o.

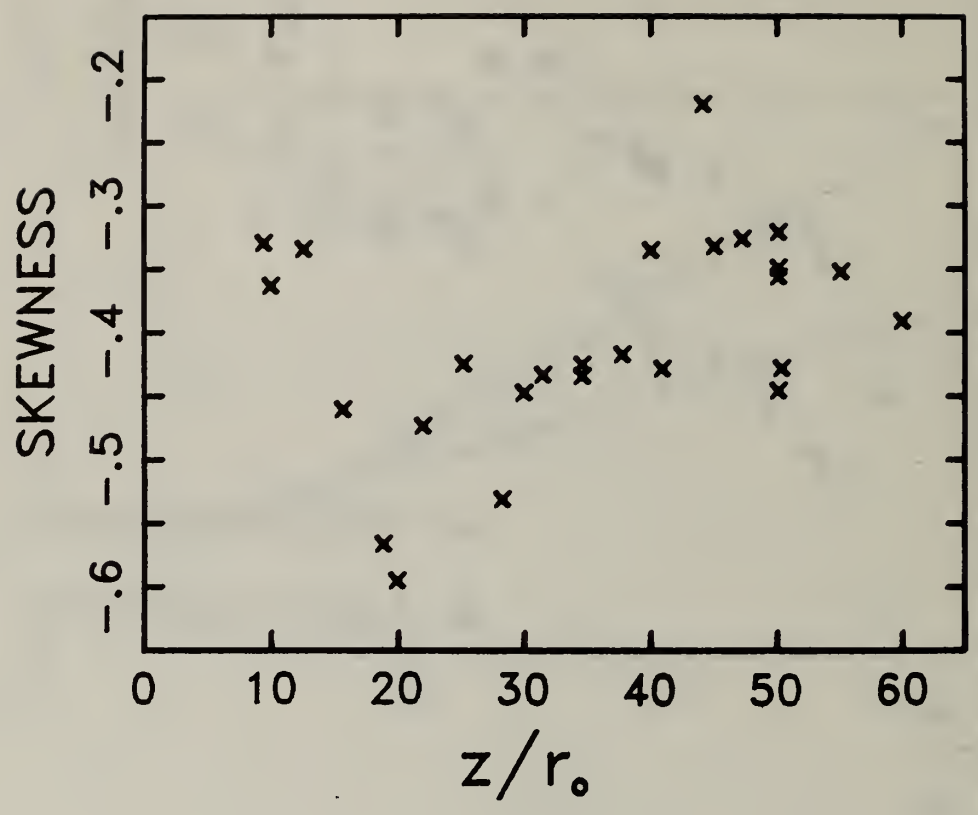

Figure 7. The skewness of the methane concentration distribution on the jet centerline is plotted as a function of z/r_o.

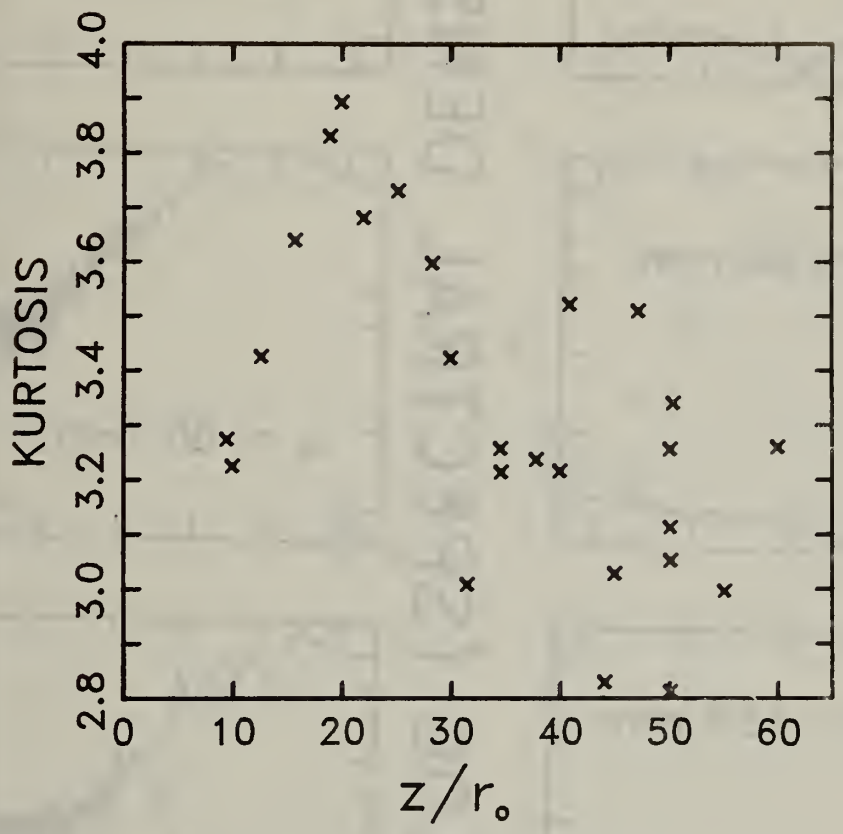

Figure 8. The kurtosis of the methane concentration distribution on the jet centerline is plotted as a function of z/r_o.

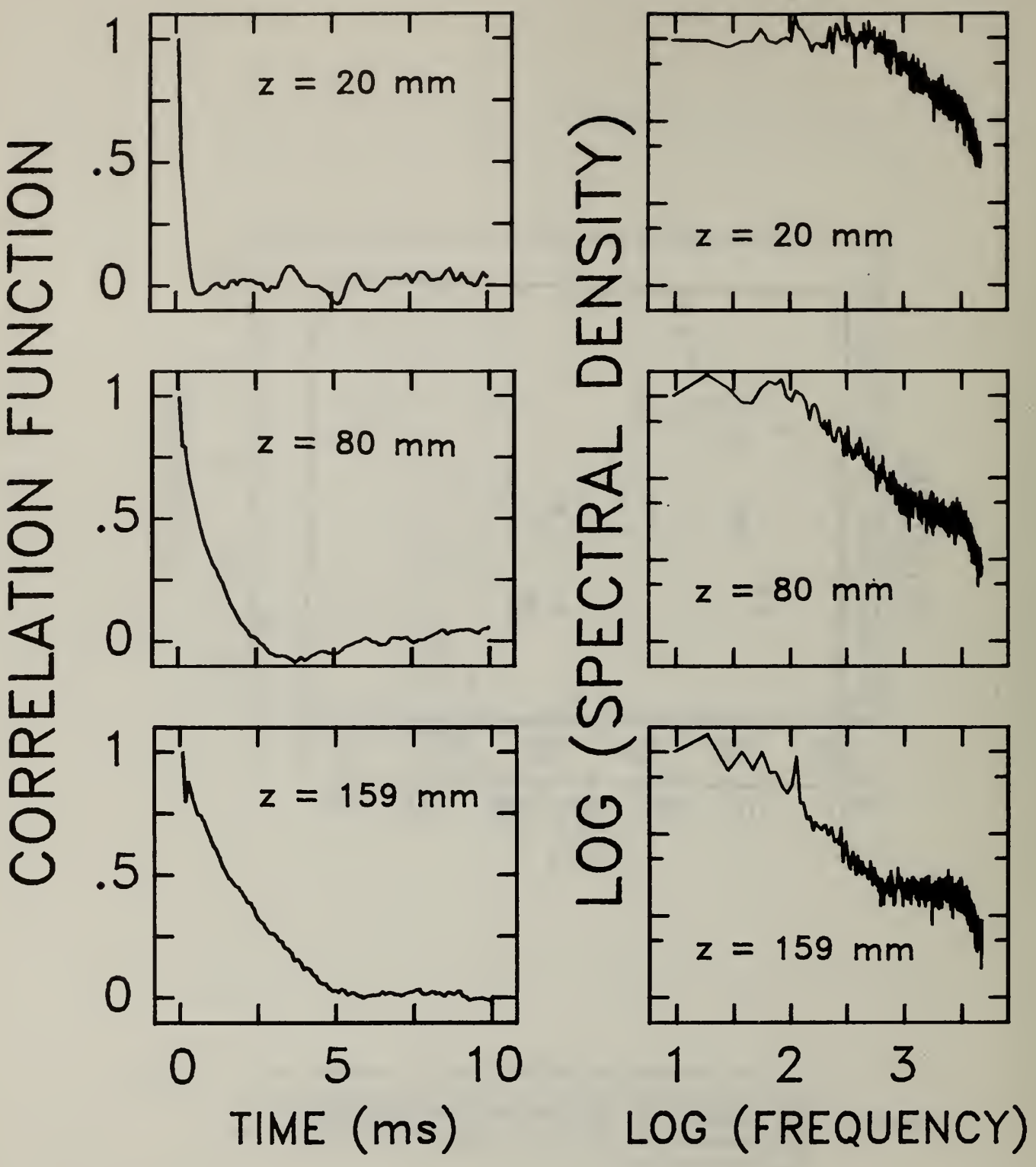

Figure 9. Examples of correlation functions and power spectra for methane concentration fluctuations at three different axial downstream distances in a methane-air jet. The cut-off frequency of the amplifier is set to 4.6 kHz.

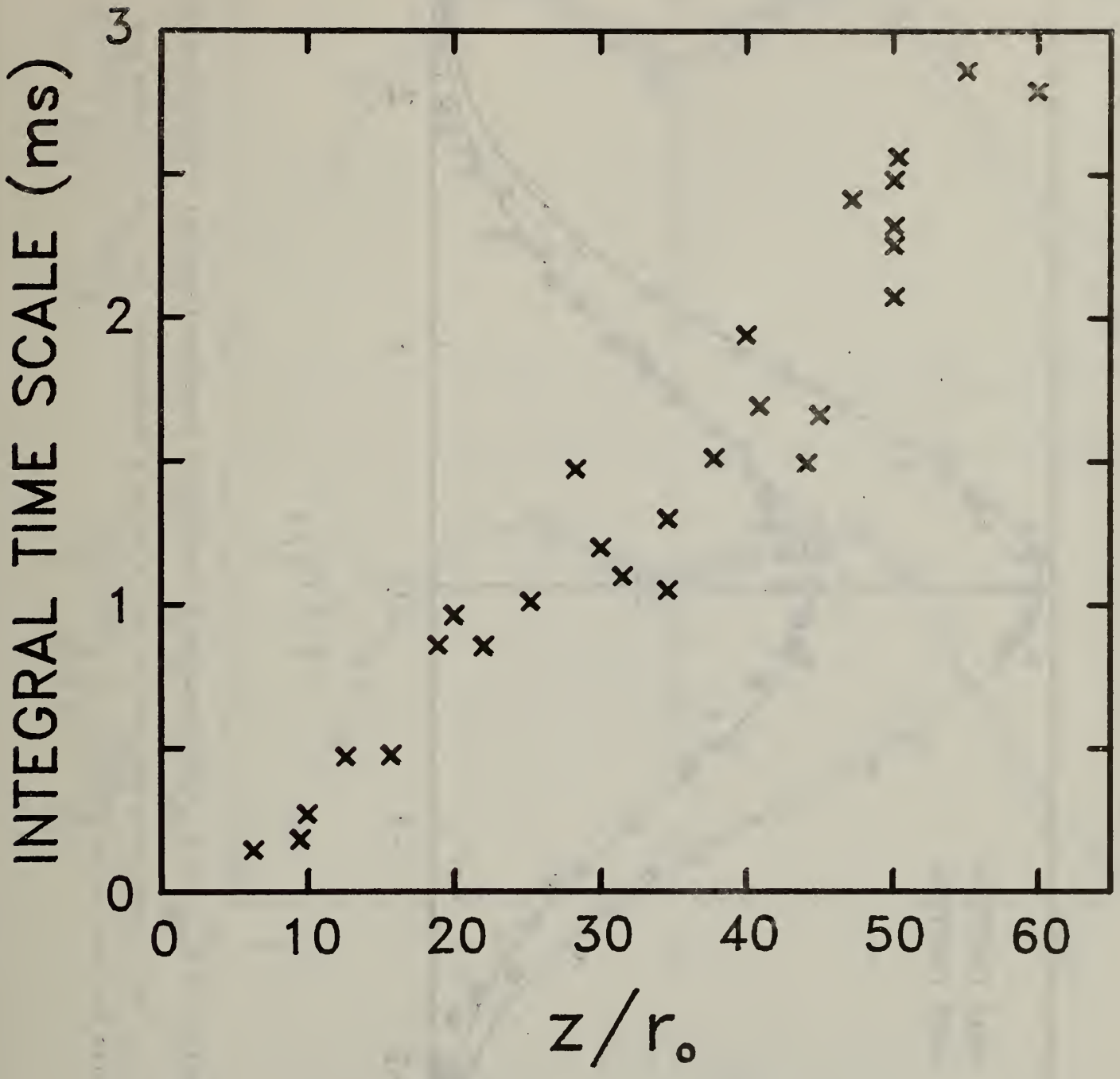

Figure 10. Integral time scales (T) on the jet centerline as a function of z/r_o.

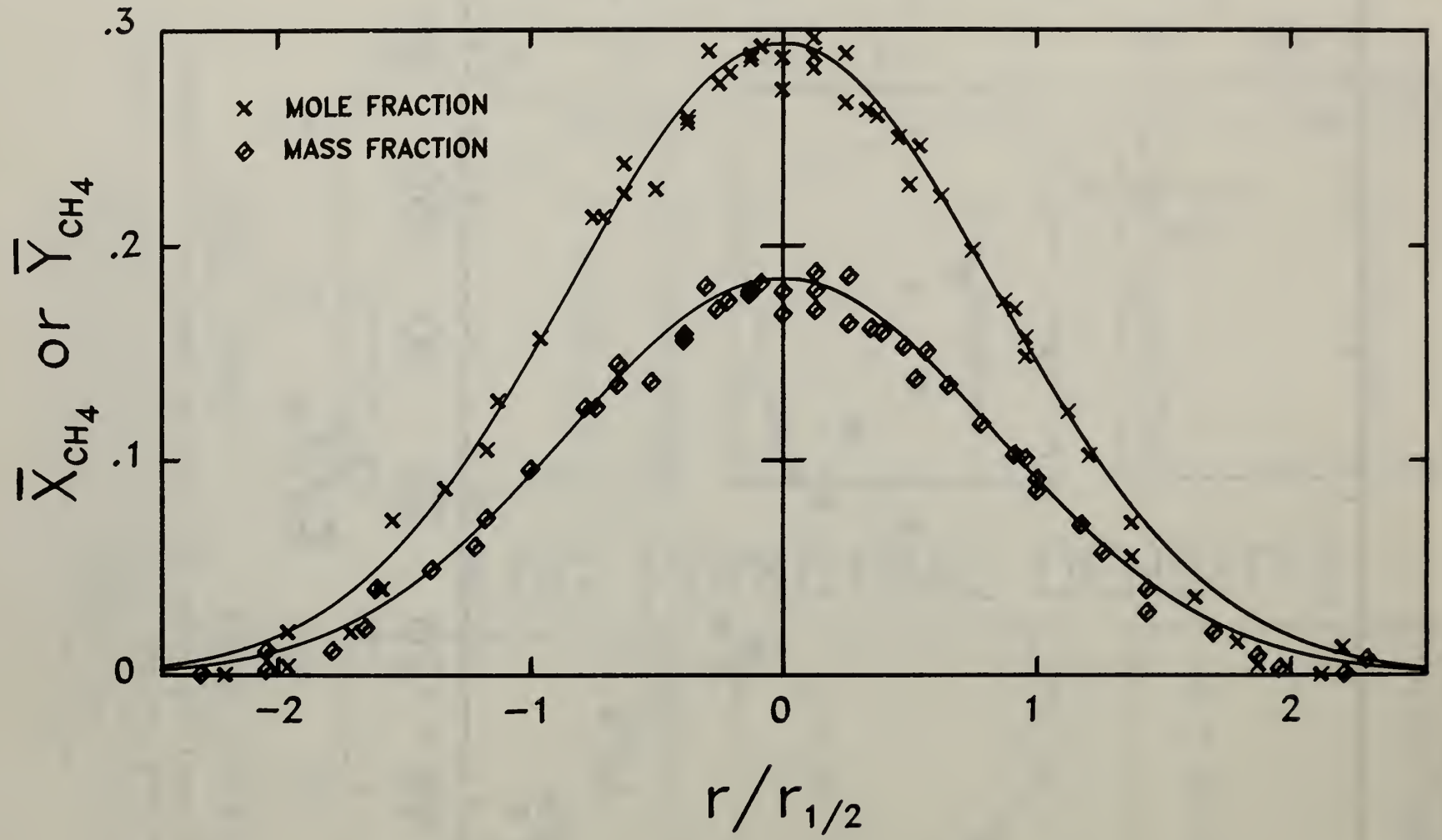

Figure 11. Behaviors of $\bar{X}_{CH_4}$ and $\bar{Y}_{CH_4}$ are shown as a function of nondimensionalized radial distance ($r/r_{1/2}$) for a downstream distance of z/r_o = 35 in a methane-air jet. Solid lines are results for fits of eq. (5.5).

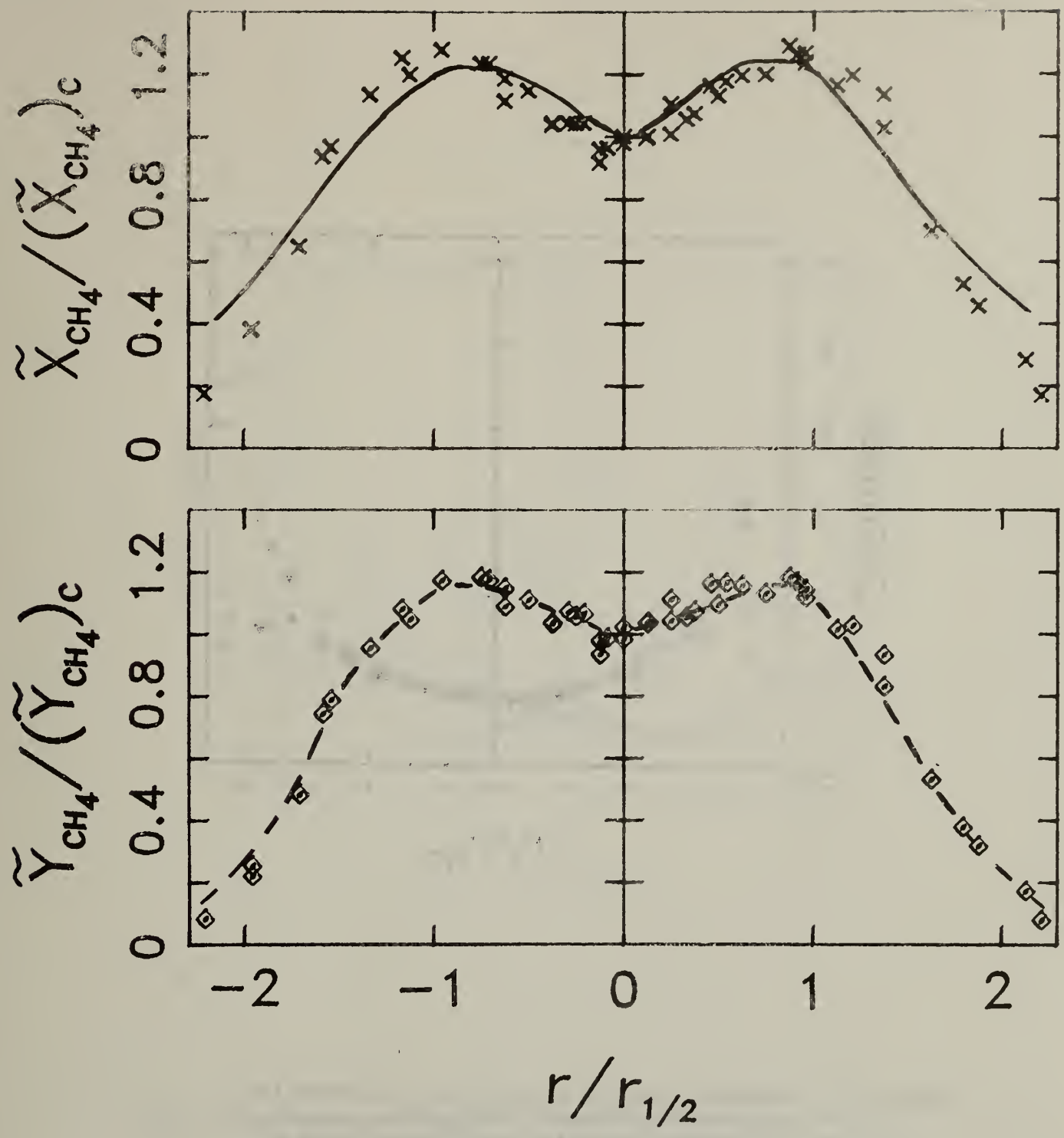

Figure 12. Experimental values of $\tilde{X}_{CH_4}/\left(\tilde{X}_{CH_4}\right)_c$ and $\tilde{Y}_{CH_4}/\left(\tilde{Y}_{CH_4}\right)_c$ are shown as a function of nondimensionlized radial distance $(r/r_{1/2})$ for a downstream distance of $z/r_o = 35$ in a methane-air jet. The solid line represents results taken from the work of Becker et al. [48] for an air-air jet and the dashed line gives the results of Birch et al. [23] for a methane-air jet.

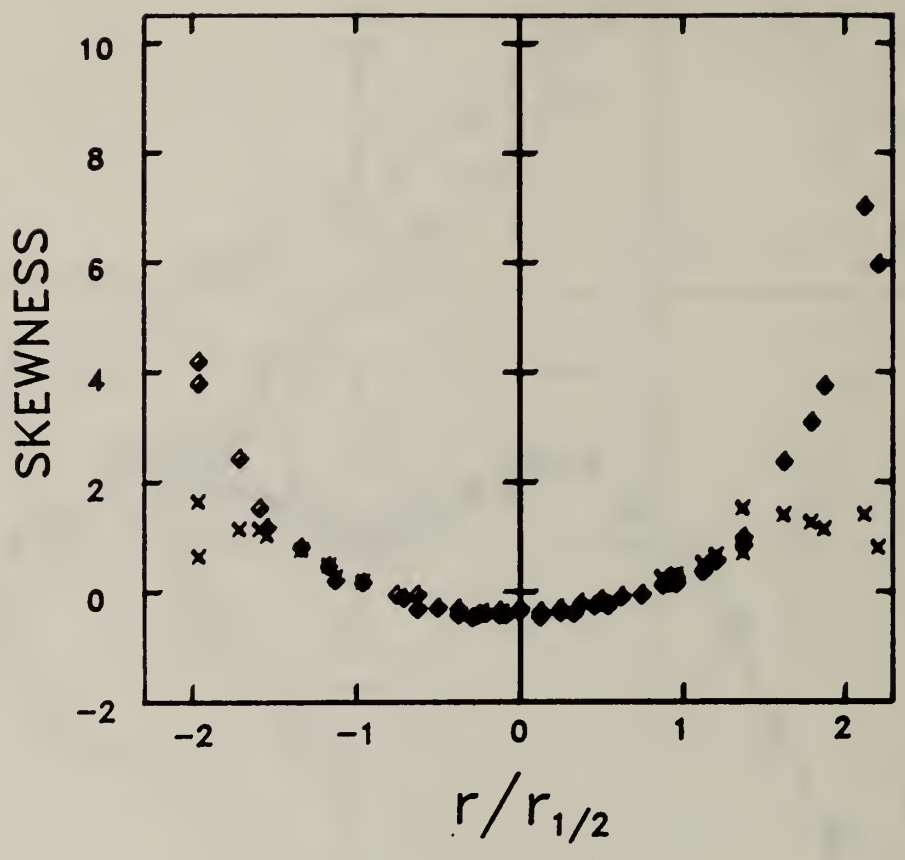

Figure 13. Skewness values as a function of nondimensionalized radial distance ($r/r_{1/2}$) are shown for the methane concentration distribution at a downstream distance z/r_o = 35 in a methane-air jet. Values have been calculated for entire data records (◈) and for conditionally sampled data which are weighted by the corresponding intermittency function (X).

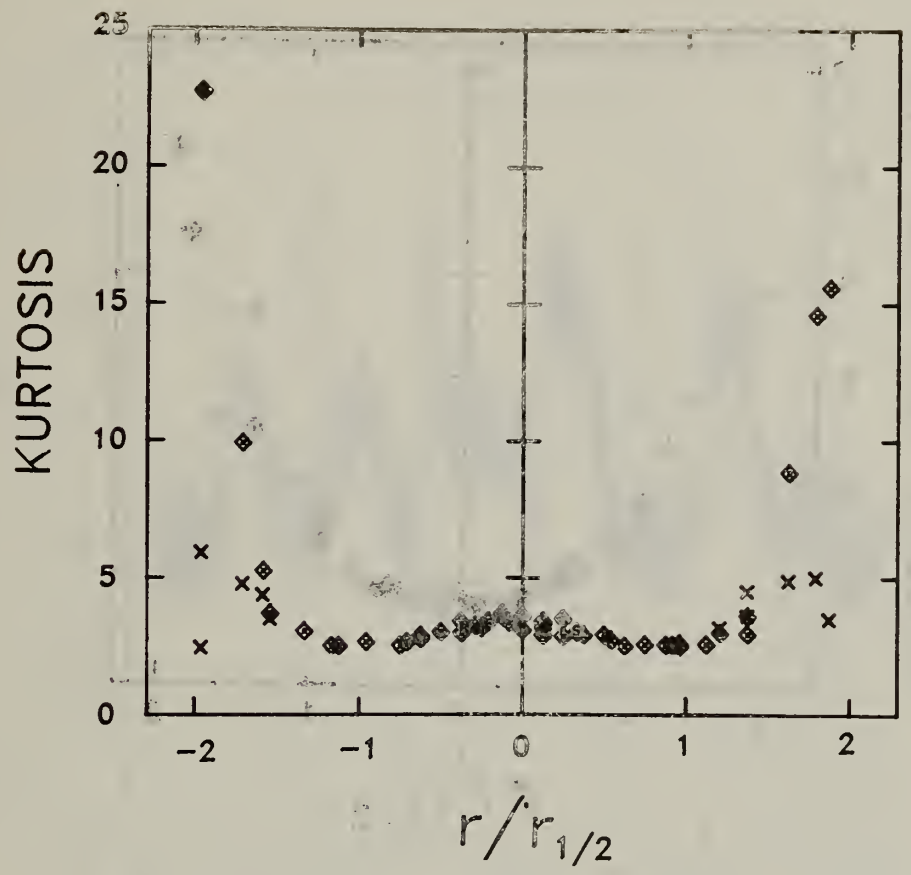

Figure 14. Kurtosis values as a function of nondimensionalized radial distance ($r/r_{1/2}$) are shown for the methane concentration distribution at a downstream distance $z/r_o = 35$ in a methane-air jet. Values have been calculated for entire data records (◈) and for conditionally sampled data which are weighted by the corresponding intermittency functions (X).

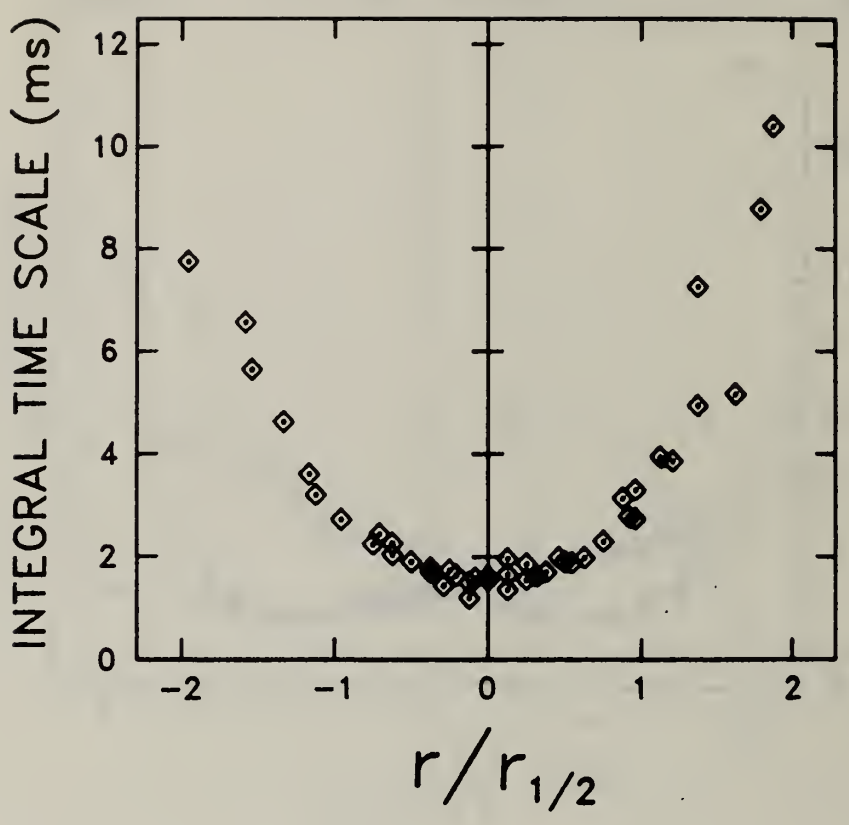

Figure 15. Integral time scales as a function of nondimensionalized radial distance ($r/r_{1/2}$) are shown for methane concentration fluctuations at a downstream distance z/r_o = 35 in a methane-air jet.

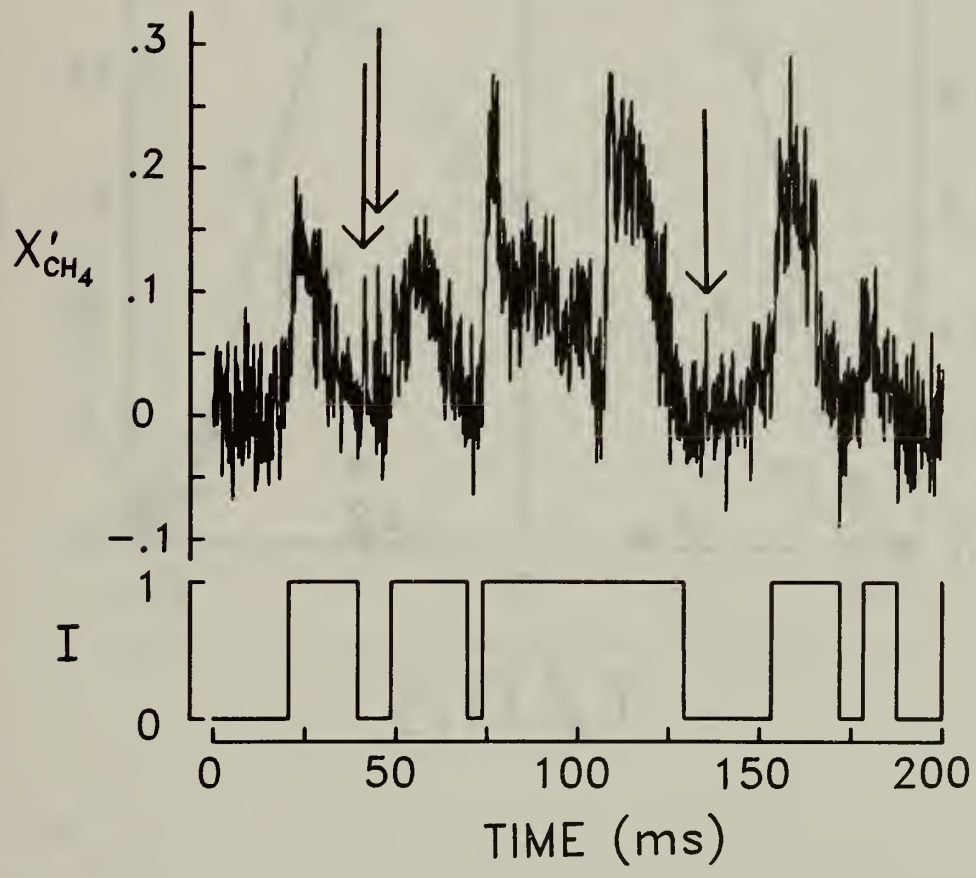

Figure 16. Examples of methane concentration behavior in the intermittent region of a methane-air jet and the resulting intermittency function calculated for the data. Arrows indicate short "bursts" of methane concentration which do not appear in the intermittency function due to the averaging inherent in the calculation of this function.

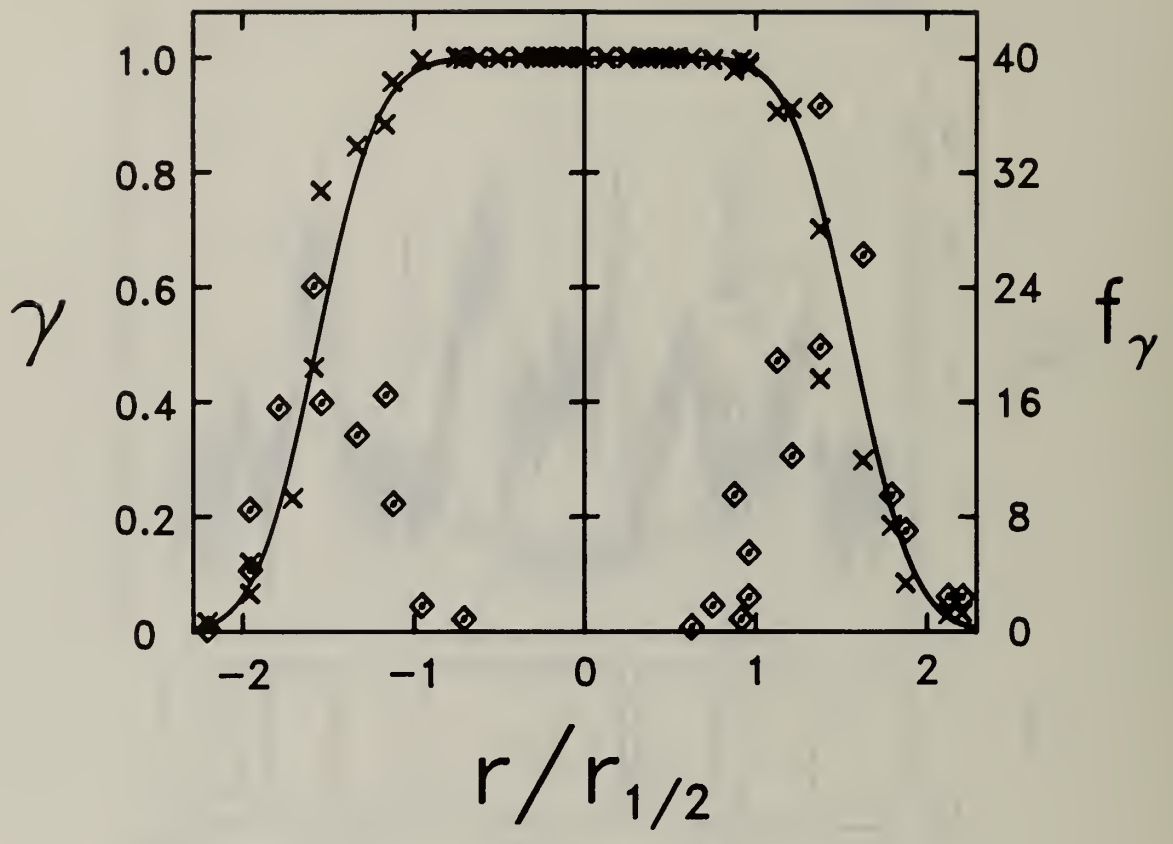

Figure 17. Intermittency factor (γ) and frequency (f_γ) as functions of nondimensionalized radial distance. ($r/r_{1/2}$) for a downstream distance of z/r_o = 35 in a methane-air jet. The solid line is a plot of Eq. (5.6) for R = 1.6 $r_{1/2}$ and σ_w = .28 $r_{1/2}$.

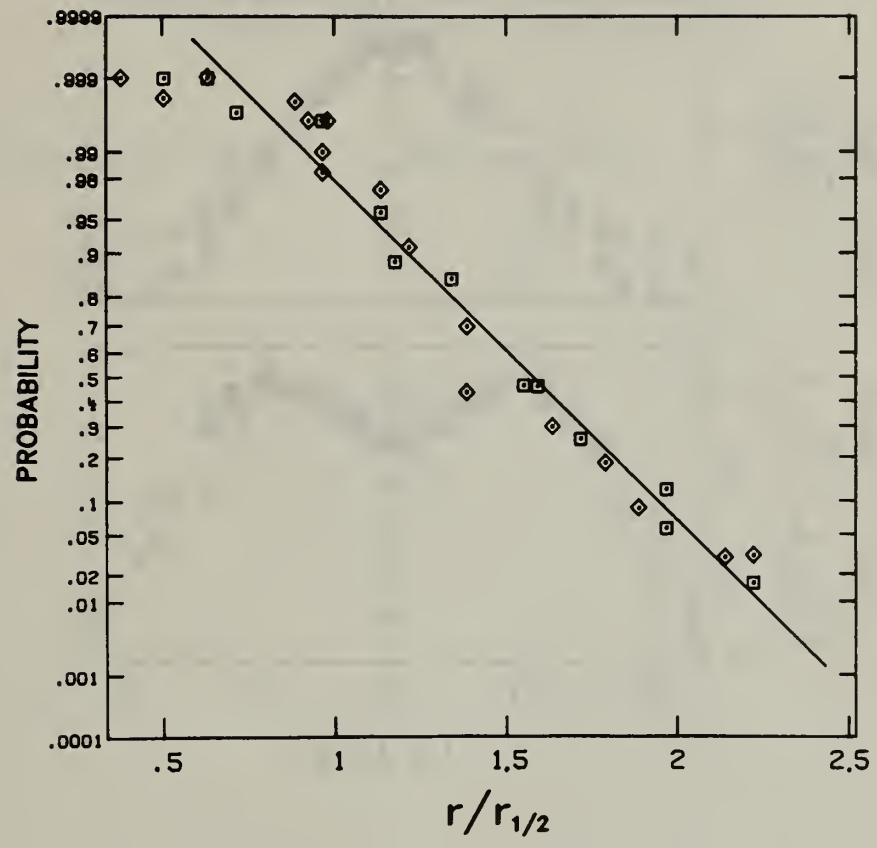

Figure 18. Values of the intermittency factor (γ) are plotted on a probability graph as a function of nondimensionalized radial distance ($r/r_{1/2}$). The solid line is a linear least square fit of all results except the five points closest to the jet centerline. The symbols refer to positive (◈) and negative (⊡) values of r.

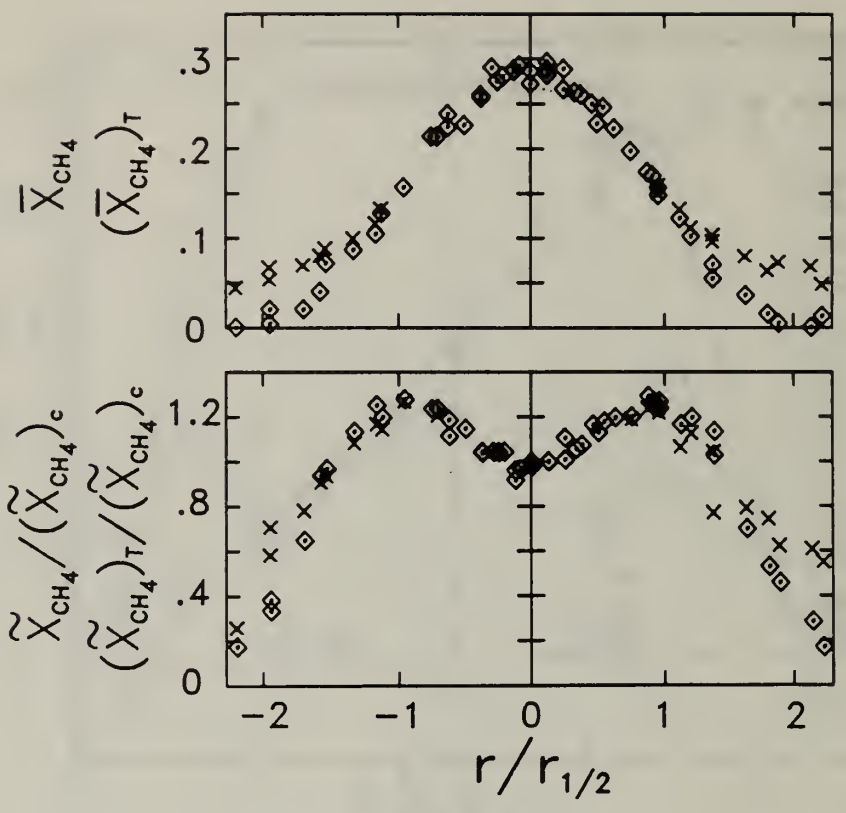

Figure 19. Plots of $\bar{X}_{CH_4}$ and $\tilde{X}_{CH_4} / \left(\tilde{X}_{CH_4}\right)_c$ are given as a function of the nondimensionalized radial distance $r/r_{1/2}$ at a downstream distance $z/r_o = 35$ in a methane-air jet. The corresponding conditionally sampled values, $\left(\bar{X}_{CH_4}\right)_T$ and $\left(\tilde{X}_{CH_4}\right)_T / \left(\tilde{X}_{CH_4}\right)_c$, are indicated by the symbol X.

Table 1. Observed and Calculated Relative Errors as a Function of Cut-off Frequency for the Current From a Photomultiplier Illuminated by a Constant Intensity Light Source

Cut-off Frequency (Hz)	Observed Relative Error	Calculated Relative Error
5700	.028	.019
2280	.017	.012
1140	.011	.009

Table 2. Experimentally Determined Constants for Eqs. (5.1)-(5.4) and Asymptotic Values for Concentration Fluctuation Intensity on the Jet Centerline in Mole and Mass Fraction Terms

Source	Jet	C_1^X	z_o^{1X}	C_1^Y	z_o^{1Y}	C_2^X	z_o^{2X}	C_2^Y	z_o^{2Y}	ζ_{Mole}	ζ_{Mass}
Present Data	CH_4-Air	0.083	$-7.5r_o$	0.112	$-2.0r_o$	0.286	$-34.8r_o$	0.569	$-11.9r_o$	0.290	0.270
Birch et al. [23]	CH_4-Air	0.090	$3.5r_o$	0.125	$11.6r_o$	-	-	0.58	$1.6r_o$	-	0.290
Dyer [2]	Propane-Air	0.114	$5.1r_o$	0.090	$0.3r_o$	-	-			-	-
Becker et al. [48]	Air-Air	0.093	$4.8r_o$	0.0925	$4.8r_o$	0.416	$-1.7r_o$	0.416	$-1.7r_o$	0.222	0.222

Table 3. Observed Constants for Spreading Rate Behavior (Eq. 6.1) of Axisymmetric Jets

Source	Jet	Concentration Units	C_3	z_o
Present Data	CH_4-Air	Mole	.108[a]	0
			.105[a]	$-9.1r_o$
		Mass	.104[a]	0
			.103[a]	$-2.0r_o$
Birch et al. [23]	CH_4-Air	Mass	.097	0
Santoro et al. [60]	10% CH_4-Air	Mole	.097[a]	0
Dyer [2]	Propane-Air	Mole	.086[a]	0
Becker et al. [48]	Air-Air	Mole	.106	$4.8r_o$

[a]From one downstream position

Table 4. Maximum Normalized RMS Concentration Fluctuation Values and Radial Locations for Various Axisymmetric Jets

Source	Jet	$\tilde{X}_{max}/\tilde{X}_c$	$\tilde{Y}_{max}/\tilde{Y}_c$	$r_{max}/r_{1/2}$
Present Data	CH_4-Air	1.31	--	0.92
	CH_4-Air	--	1.18	0.70
Birch et al. [23]	CH_4-Air	--	1.20	0.7
Becker et al. [48]	Air-Air	1.15	1.15	0.8
Shaughnessy & Morton [16]	Air-Air	1.14	1.14	0.9
Antonia et al. [50]	Air-Air	1.19	1.19	1.0
Chevray & Tutu [51]	Air-Air	1.21	1.21	0.95
Dyer [2]	Propane-Air	1.19	--	0.7
	Propane-Air	--	1.29[a]	0.8[a]

[a]Calculated from mole fraction data given in paper

Table 5. Experimental Parameters for Different Jets Discussed in Text

Source	Jet	ρ_{Jet}/ρ_{Air}	u_{Air}/u_{Jet}	Re
Present Work	CH_4-Air Axisymmetric	0.55	0.026	3770
Birch et al. [23]	CH_4-Air Axisymmetric	0.55	0	16,000
Santoro et al. [60]	10% CH_4-Air Axisymmetric	0.96	0	29,000
Dyer [2]	Propane-Air Axisymmetric	1.52	0.033	9470
Becker et al. [48]	Air-Air Axisymmetric	1.0	0	54,000
Shaughnessy & Morton [16]	Air-Air Axisymmetric	1.0	0.024 0.042	56,000 31,500
Antonia et al. [50]	Heated Air-Air Axisymmetric	0.94	0.15 0.34 0.53	32,000 25,000 18,000
Chevray & Tutu [51]	Heated Air-Air Circular	0.94	0	34,100

NBS-114A (REV. 2-80)

U.S. DEPT. OF COMM. BIBLIOGRAPHIC DATA SHEET (See instructions)	1. PUBLICATION OR REPORT NO. NBSIR 83-2641	2. Performing Organ. Report No.	3. Publication Date February 1983

4. TITLE AND SUBTITLE

The Application of Laser-Induced Rayleigh Light Scattering to the Study of Turbulent Mixing

5. AUTHOR(S)

William Pitts and Takashi Kashiwagi

6. PERFORMING ORGANIZATION (If joint or other than NBS, see instructions)

NATIONAL BUREAU OF STANDARDS
DEPARTMENT OF COMMERCE
WASHINGTON, D.C. 20234

7. Contract/Grant No.

8. Type of Report & Period Covered

9. SPONSORING ORGANIZATION NAME AND COMPLETE ADDRESS (Street, City, State, ZIP)

10. SUPPLEMENTARY NOTES

☐ Document describes a computer program; SF-185, FIPS Software Summary, is attached.

11. ABSTRACT (A 200-word or less factual summary of most significant information. If document includes a significant bibliography or literature survey, mention it here)

This work describes the development and characterization of an experimental system employing laser-induced Rayleigh light scattering with digital data acquisition as a time-resolved, quantitative concentration probe in the turbulent flow field of a binary gas mixture. Equations for the expected signal and noise levels are given. Estimates of these parameters for the experimental system used here are in satisfactory agreement with experiment. It is demonstrated the laser Rayleigh light scattering technique does provide highly spatially- and time-resolved measurements within the concentration flow field. Measurements at various postions in the flow field of an axisymmetric methane jet issuing into a slow flow of air are reported and where possible, compared with appropriate literature results. The statistical properties of the turbulent concentration fluctuations are found to be in good agreement with other independent measurements. Conditionally sampled measurements are also reported and shown to behave in the same manner as the limited number of similar measurements in the literature. The capability of calculating power spectra and correlation functions for the time behavior of the methane concentration is also demonstrated. Other techniques employed for scalar measurements in turbulent flow fields are briefly reviewed and the utility of these techniques for measurements in different types of flow systems are discussed in relation to the Rayleigh light scattering method.

12. KEY WORDS (words by semicolons)

Axisymmetric jet; concentration flow field; intermittency; laser; ramp-like structures; Rayleigh light scattering; scalar probe; turbulence; turbulent flow

13. AVAILABILITY

☒ Unlimited

☐ For Official Distribution. Do Not Release to NTIS

☐ Order From Superintendent of Documents, U.S. Government Printing Office, Washington, D.C. 20402.

☒ Order From National Technical Information Service (NTIS), Springfield, VA. 22161

14. NO. OF PRINTED PAGES 114

15. Price $13.00

USCOMM-DC 6043-P80